

**CUSTOM DEVICE FOR LOW-DOSE GAMMA IRRADIATION OF
BIOLOGICAL SAMPLES**

A Thesis

by

RUOMING BI

Submitted to the Office of Graduate Studies of
Texas A&M University
in partial fulfillment of the requirements for the degree of

MASTER OF SCIENCE

December 2011

Major Subject: Health Physics

**CUSTOM DEVICE FOR LOW-DOSE GAMMA IRRADIATION OF
BIOLOGICAL SAMPLES**

A Thesis

by

RUOMING BI

Submitted to the Office of Graduate Studies of
Texas A&M University
in partial fulfillment of the requirements for the degree of

MASTER OF SCIENCE

Approved by:

Chair of Committee,	John R. Ford
Committee Members,	John W. Poston, Sr.
	Michael A. Walker
Head of Department,	Raymond J. Juzaitis

December 2011

Major Subject: Health Physics

ABSTRACT

Custom Device for Low-Dose Gamma Irradiation of Biological Samples.

(December 2011)

Ruoming Bi, B.S., Texas A&M University

Chair of Advisory Committee: Dr. John Ford

When astronauts travel in space, their primary health hazards are high-energy cosmic radiations from galactic cosmic rays (GCR). Most galactic cosmic rays have energies between 100 MeV and 10 GeV. For occupants inside of a space shuttle, the structural material is efficient to absorb most of the cosmic-ray energy and reduce the interior dose rate to below 1.2 mGy per day. However, the biological effects of prolonged exposure to low-dose radiation are not well understood. The purpose of this research was to examine the feasibility of constructing a low-dose irradiation facility to simulate the uniform radiation field that exists in space. In this research, we used a pre-manufactured incubator, specifically the Thermo Scientific Forma Series II Water Jacketed CO₂ Incubator, to act as shielding and simulate the exterior of the space shuttle. To achieve the desired dose rate (< 1 mGy/h) inside the incubator volume, the computer code MCNPX was used to determine required source activity and distance between the shielding and source. Once the activity and distance were calculated, an experiment was carried out to confirm the simulation results, which used survey meters and thermoluminescence dosimeters (TLDs) to map the radiation field within the incubator.

Based on results from the MCNPX simulation and the actual experiment, a uniform radiation field was achieved in the rear space of the incubator, which accounted for the majority of the incubator volume. Furthermore, the actual dose rate had a range from 0.298 to 0.696 mGy/h, hence meeting the initial design criteria.

ACKNOWLEDGEMENTS

This research was supported by the Center for Bio-nanotechnology and Environmental Research at Texas Southern University as part of a NASA research grant.

I would like to thank my committee chair, Dr. John Ford, and my committee members, Dr. John Poston and Dr. Michael Walker, for their guidance and support throughout the course of this research. I would also like to thank all the people of the Nuclear Science Center at Texas A&M University, particularly Dr. Warren Reece and Dr. Latha Vansudevan, for their efforts assisting me to complete this research. I would like to thank all my friends, especially Fada Guan for giving me valuable MCNP support, and Shaoyong Feng for proofreading. Finally, I thank my family members for their love and encouragement.

NOMENCLATURE

GCR	Galactic Cosmic Ray
LET	Linear Energy Transfer
RBE	Relative Biological Effectiveness
MCNP	Monte Carlo N-Particle
MCNPX	Monte Carlo N-Particle eXtension
TLD	Thermoluminescence Dosimeters
HVL ₁	First Half-Value Layers
HVL ₂	Second Half-Value Layers
HC	Homogeneity Coefficient
h _v _{eq}	Equivalent Photon Energy

TABLE OF CONTENTS

	Page
ABSTRACT	iii
ACKNOWLEDGEMENTS	v
NOMENCLATURE	vi
TABLE OF CONTENTS	vii
LIST OF FIGURES	ix
LIST OF TABLES	xii
I INTRODUCTION	1
I. A Cosmic Rays.....	1
I. B Radiation Dose for Astronauts.....	2
I. C Previous Designs of Low Dose Rate Irradiation Facilities.....	4
I. D Thermoluminescence Detector (TLD).....	9
I. E TLD Reader	10
I. F Gamma Interactions in Matter.....	11
I. G X-Ray Beam Quality Specification	12
I. H Relative Error	13
II MODELS AND METHODS	14
II. A Overall Design.....	14
II. B Source.....	16
II. C Shielding.....	20
II. D Distance.....	23
III MEASUREMENTS AND SIMULATION.....	25
III. A TLD	25
III. B MCNPX Simulation.....	37
IV DISCUSSION	54

	Page
V CONCLUSION AND FUTURE WORK	58
V.A Conclusion	58
V.B Future work.....	58
REFERENCES	60
APPENDIX A	62
APPENDIX B.....	65
APPENDIX C.....	66
APPENDIX D	67
APPENDIX E.....	70
APPENDIX F	76
VITA.....	82

LIST OF FIGURES

FIGURE	Page
I.1 Primary cosmic ray energy spectrum (Mishev et al. 2004).....	2
I.2 Schematic of irradiator system constructed by University of Medicine and Dentistry of New Jersey-New Jersey Medical School (Howell et al. 1997)	6
I.3 Schematic of experiment conducted by Sakai et al. 2003.	7
I.4 Typical low dose irradiation facility, Tokyo, Japan (Sakai et al. 2003).....	7
I.5 MIT liquid source irradiator (Olipitz et al. 2010).	8
I.6 Schematic of a basic TLD reader	10
I.7 Relative importance of the three common gamma interaction types	11
II.1 Top view of irradiation system	15
II.2 Photo of the actual experiment setup	15
II.3 Co-60 neutron activation schematic	17
II.4 The activity of an activator detector with respect to time	20
II.5 Thermo Scientific Forma Series II Water Jacketed CO ₂ Incubator	21
II.6 Simplified incubator diagram with bacteria culture vessel.....	23
III.1 TLD locations within the incubator.....	25
III.2 Equivalent photon energy vs. HVL ₁ in copper or aluminum (Attix 2004)	27
III.3 Thermoluminescent response of LiF for photon energy from 6 to 2800 keV (Attix 2004).....	28
III.4 Glow curve of TLD #1 after exposure to 0.786 R X-ray	30
III.5 Glow curve of TLD #3 after exposure to 0.786 R X-ray	31

FIGURE	Page
III.6 Glow curve of TLD #4 after exposed to 0.786 R X-ray.....	31
III.7 XY cross section of the irradiation system.....	38
III.8 XZ cross section of the irradiation system	38
III.9 XY cross section of the irradiation system with photon paths.....	39
III.10 XZ cross section of the irradiation system with photon paths	39
III.11 Gamma fluence distribution in Plane A	42
III.12 Gamma fluence distribution in Plane B.....	42
III.13 Gamma fluence distribution in Plane C.....	43
III.14 Gamma fluence distribution in Plane D	43
III.15 Gamma fluence distribution in Plane E.....	44
III.16 Gamma fluence distribution in Plane F	44
III.17 Gamma fluence distribution in Plane G	45
III.18 Distribution of averaged absorbed dose from single source photon in Plane A.....	48
III.19 Distribution of averaged absorbed dose from single source photon in Plane B	49
III.20 Distribution of averaged absorbed dose from single source photon in Plane C.....	49
III.21 Distribution of averaged absorbed dose from single source photon in Plane D.....	50
III.22 Distribution of averaged absorbed dose from single source photon in Plane E	50
III.23 Distribution of averaged absorbed dose from single source photon in Plane F	51

FIGURE	Page
III.24 Distribution of averaged absorbed dose from single source photon in Plane G.....	51

LIST OF TABLES

TABLE	Page
I.1 Recorded dose rate of recent NASA space programs	4
II.1 Neutron activation parameters for several materials	18
II.2 Specifications of Thermo Scientific Forma Series II Water Jacketed CO ₂ Incubator	22
III.1 Calibration filtration metal thicknesses and exposures	26
III.2 TLD calibration results after exposure to 0.786 and 1.086 R x-ray with equivalent photon energy of 160 keV	29
III.3 Modified TLD calibration results.....	32
III.4 Results of seven different exposures measured in nanocoulombs (nC).....	33
III.5 Results of seven different exposures measured in roentgens (R)	34
III.6 Absorbed dose of seven TLD exposures	35
III.7 Summary of reactor operations from 6/14/10 to 7/12/10	36
III.8 Corrected absorbed dose of seven TLD exposures	37
III.9 Conversion coefficients for air kerma per unit fluence (K_a/ϕ_a) for monoenergetic photons.....	47
III.10 MCNPX simulation of averaged absorbed dose from single source photon at various locations	52
III.11 Comparison of MCNPX simulation and measured results of total absorbed dose in eight hours.....	53
IV.1 Comparison of total absorbed dose between frontal and rear TLDs for the actual experiment and simulation.....	55

I. INTRODUCTION

I.A Cosmic Rays

Cosmic rays may broadly be divided into two categories: primary cosmic rays and secondary cosmic rays. Primary cosmic rays are energetic particles from extra-terrestrial origin that constantly bombard earth's atmosphere. They consist of about 90% high-energy protons, 9% helium and other heavier nuclei and a small percentage of electron and gamma rays (Becker, et al. 2007). As they propagate, primary cosmic rays can interact with interstellar medium to generate secondary cosmic rays. The ratio of secondary/primary nuclei is highly dependent upon the primary nuclei energy (E). According to NASA, the ratio of secondary to primary nuclei is observed to decrease approximately as $E^{-0.5}$ with increasing energy (Simpson 1983).

Like other ionizing radiation, cosmic rays, especially galactic cosmic rays (GCR), pose a significant health risk for astronauts on interplanetary missions due to their energetic nature. GCR have a wide range of energies, usually from 10^9 eV (1 GeV) to 10^{20} eV (10^8 TeV). For comparison, the most powerful man-made particle accelerators currently can only produce 10^{13} eV. The number of cosmic rays with energies beyond 1 GeV decreases by about a factor of 50 for every factor of 10 increase in energy (Mishev et al. 2004). The primary cosmic ray spectrum is shown in Figure I.1.

This thesis follows the style of Health Physics.

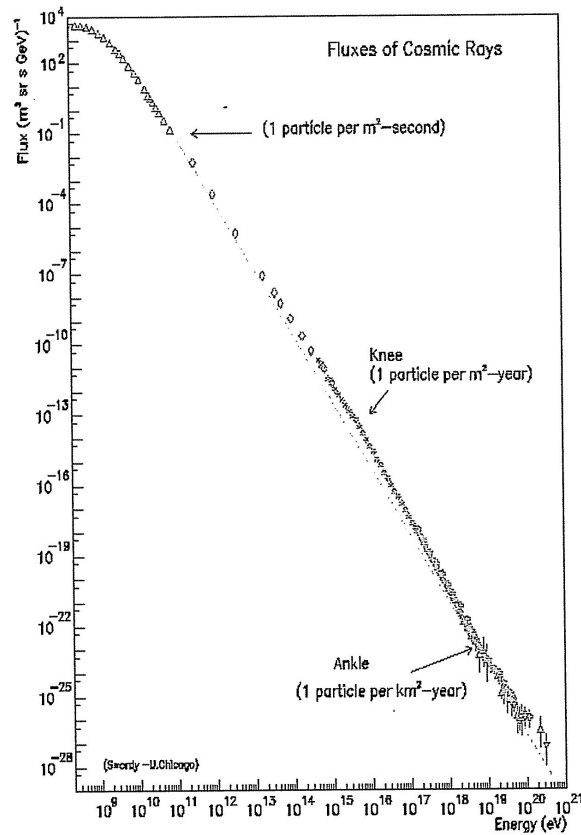


Figure I.1. Primary cosmic ray energy spectrum (Mishev et al. 2004).

I.B Radiation Dose for Astronauts

The absorbed dose (D) is defined as the amount of energy deposited in bulk material, which is commonly expressed as the product of particles fluence (F) and linear energy transfer (L) as shown in Equation 1.

$$D = F * L \quad (1)$$

Relative biological effectiveness (RBE) is used to relate the risks of different particles to the human body, which is defined as the ratio of the dose of gamma rays to the radiation under study that will produce an equal level of effect. To represent the knowledge of RBE, radiation weighting factors (W_R) were assigned to different kind of radiations. As shown in Equation 2, dose equivalent (H) is defined as the product of absorbed dose and radiation weighting factor.

$$H = D * W_R \quad (2)$$

To evaluate the organ dose or organ dose equivalent, the dose or dose equivalent are summed over the LET spectra at the tissue of interest.

The amount of radiation dose received by astronauts depends on orbital inclination, altitude, position in the solar cycle and mission duration (Cucinotta 2010). Nevertheless, absorbed doses or dose rates were recorded by dosimetry badges worn by astronauts for each NASA space mission. A summary of recent NASA space programs and their corresponding doses is shown in Table I.1.

Table I.1. Recorded dose rate of recent NASA space programs (Cucinotta 2010)

<i>NASA Program</i>	<i>No. Crew</i>	<i>D, mGy</i>	<i>E, mSv</i>	<i>D-rate, mGy/d</i>	<i>E-rate, mSv/d</i>
Mercury	6	0.1	0.15	0.3	0.55
Gemini	20	1.3	2.2	0.49	0.87
Apollo	33	4.1	12.0	0.43	1.2
Skylab (50 deg x 430 km)	9	40.3	95.0	0.71	1.4
ASTP (50 deg x 220 km)	3	1.1	2.3	0.12	0.26
STS 28.5 deg (>400 km)	85	9.5	17.0	1.2	2.1
28.5 deg (< 400 km)	207	0.9	1.6	0.1	0.18
39-40 deg	57	1.1	2.4	0.1	0.21
>50 deg (>400 km)	10	2.2	5.2	0.44	1.1
>50 deg (<400 km)	190	1.7	3.8	0.2	0.45
NASA-Mir (51.6 deg x 360 km)	6	50.3	115	0.37	0.84
ISS Exp.'s 1-10 (51.6 deg x 380 km)	13	26.0	68.0	0.16	0.40

I.C Previous Designs of Low Dose Rate Irradiation Facilities

Although the linear non-threshold model is a widely accepted hypothesis in current radiation protection practices, the biological effects of prolonged exposure due to low-dose radiation are not well understood. According to the National Radiological Protection Board (NRPB), the terms of "low dose" and "low dose rate" are defined as below 100 mGy and below 5 mGy per hour (Wakeford and Tawn 2010).

As early as the 1970s, health physicists attempted to study the effects of ionizing radiation on plants and animals under natural conditions by constructing several large scale outdoor irradiators. Amongst the many, two facilities located in Canada were the

most noticeable due to their size and irradiation duration. The Field Irradiator - Gamma (FIG) was designed to monitor the effects of a fixed gradient of gamma radiation on a boreal forest. It was used for 14 years to study plant community ecology. Its animal counterpart, the zoological environment under stress (ZEUS) facility, was used for 4 years to study small mammal health and population (Mihok 2004). Ecological results from such large scale field experiment provided valuable data to develop a practical system for environmental protection (ICRP 2003). However, large outdoor irradiators faced statistical and methodological difficulties when smaller sample sizes were selected for more in-depth studies. For this reason, more modern studies favor smaller indoor facilities.

Several experiments were conducted in 2008 at Chalk River Laboratories, Canada, to simulate potential occupational exposure by exposing mice to chronic low-dose gamma radiation. In such experiments, unrestrained mice in their plastic cages were irradiated with a Co-60 open beam source (GammaBeam 150, Atomic Energy of Canada Limited). Animals were exposed daily to about 0.33 mGy of gamma radiation delivered at low dose rate (0.7 mGy/h), and the exposure was repeated 5 days per week for a duration up to 90 weeks. Activity lost to decay over this extended period was compensated by regularly adjusting the distance between the source and the animals to maintain the stated daily dose and dose rate (Mitchel et al. 2008).

Using the same principle of dose-to-distant relationship, more advanced irradiator prototypes were built. One of the prototypes was constructed at the New Jersey Medical School, which coupled a computer controlled variable mercury attenuator with

a cesium-137 irradiator. The operator could control the target dose rate by introducing a layer of mercury between source and cages from the mercury attenuator while keeping source activity constant. This system could accommodate six cages placed at different distances from the source, hence, achieving different target dose rates. A schematic of this irradiator system is shown in Figure I.2.

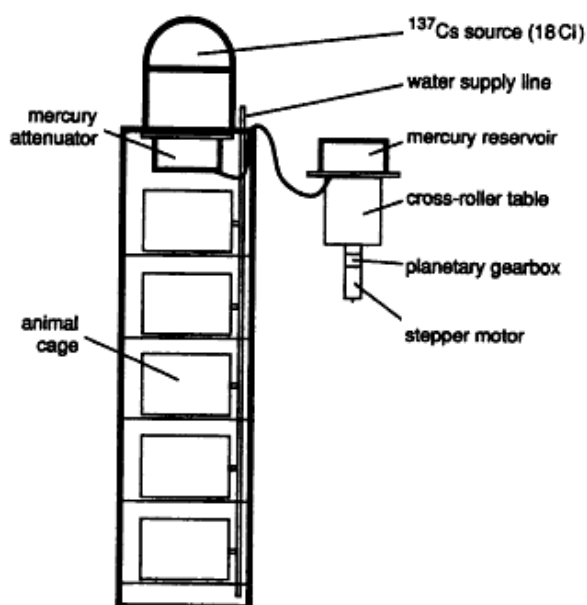


Figure I.2. Schematic of irradiator system constructed by University of Medicine and Dentistry of New Jersey-New Jersey Medical School (Howell et al. 1997).

South Korea (Shin et al. 2010) and Japan (Ishida et al. 2010) have also conducted comparable research experiments to study the effect of low-dose radiation by converting the entire room into an irradiation chamber. As shown in Figure I.3 and I.4, the experiments use distance as the sole means to modify dose rate by placing test subjects at defined distances from a single source (Sakai et al. 2003).

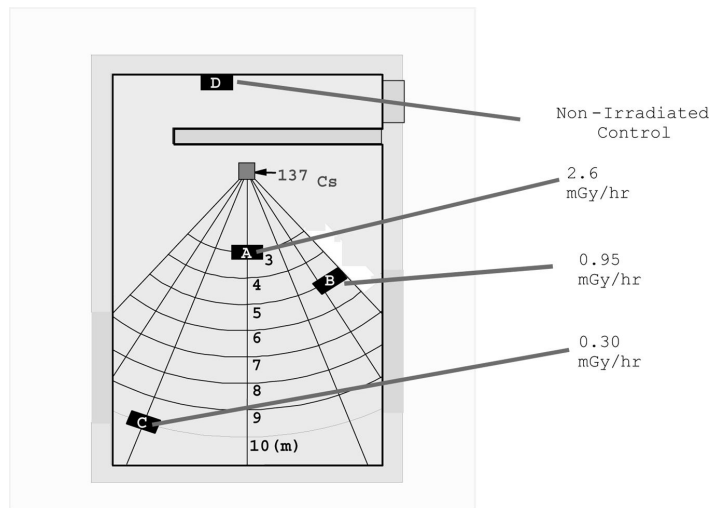


Figure I.3. Schematic of experiment conducted by Sakai et al. 2003.



Figure I.4. Typical low dose irradiation facility, Tokyo, Japan (Sakai et al. 2003).

Because dose rate at a given location is inversely proportional to the square of distance, location further away from the source is bound to have lower dose rate. Due to this asymmetrical nature, radiation field uniformity cannot be achieved for single source irradiators. To combat this drawback, an irradiator system was constructed at the

Massachusetts Institute of Technology (MIT), which used liquid radioactive source. The liquid was made by mixing varying activities of I-125 into a sodium hydroxide (NaOH) solution to maintain the desired dose rate. Shown in Figure I.5, the irradiator consisted a plastic cart (PC) holding an aluminum tray (T) and a flood phantom (P). The phantom was filled with radioactive liquid and served as radiation source. A steel cart (SC) holding the cages fits exactly above the plastic cart. A leaded acrylic sheet (A) was mounted on the steel cart to ensure radiation protection for experimenters (Olipitz 2010).

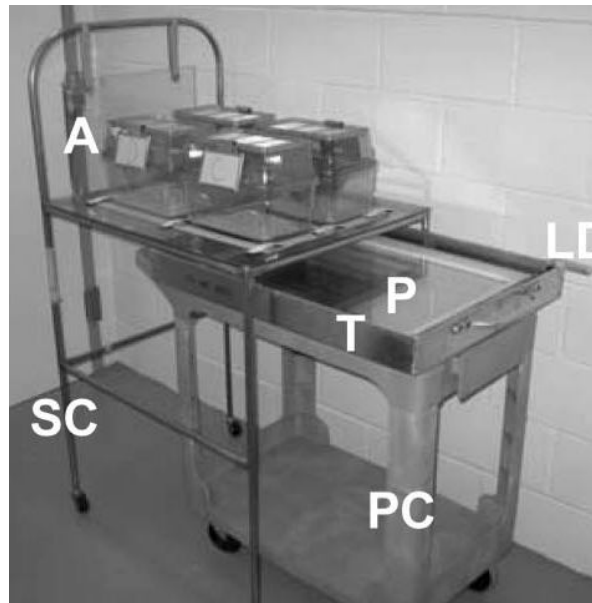


Figure I.5. MIT liquid source irradiator (Olipitz et al. 2010).

The MIT irradiator design was an advancement over one-source irradiator designs, however, it did not entirely solve the problem because dose rates at higher altitudes were still lower than the base, where the source was located. For this reason, it

is necessary to examine the feasibility of constructing a uniform low-dose irradiation facility for the future experiments.

I.D Thermoluminescence Detector (TLD)

A TLD is a type of passive dosimeter which is used to measure exposure from ionizing radiation. They were chosen to be used in this research due to their low energy dependence, high sensitivity and stability. There are three frequently used LiF-based TLDs for dose monitoring purposes, namely TLD-100 (natural lithium, 92.6% Li-7, 7.4% Li-6), TLD-600 (95.62% Li-6) and TLD-700 (99.993% Li-7). TLD-100 and TLD-600 are commonly used for gamma and thermal neutron detection due to their lithium-6 concentration. This is because thermal neutrons are detected through the (n, α) reaction, and lithium-6 has a cross section equal to 950 b for thermal energies. On the other hand, TLD-700 contains enriched lithium-7 and is only sensitive to gamma due to the small neutron cross section (0.033 b for thermal neutron) (Tsoulfanidis 1995). Because cobalt-60 was used as radiation source, TLD-700 was chosen for use in this research.

Structurally, a TLD is a phosphor produced by hot-pressing crystals of a TLD powder into a solid form. When a TLD is exposed to ionizing radiation at ambient temperatures, the radiation interacts with the phosphor and deposits all or part of the incident energy in that material. Some of the atoms in the material that absorb that energy become ionized, producing free electrons and areas lacking one or more electrons, called holes. Imperfections in the crystal lattice structure act as sites where free electrons can become trapped and held in place.

To read the TLD chip, heating is required. Heating the crystal causes the crystal lattice to vibrate, releasing the trapped electrons in the process. Released electrons return to the original ground state, releasing the captured energy from ionization as light, hence the name thermoluminescent. Released light is measured using a photomultiplier tube and the number of photons counted is proportional to the quantity of radiation striking the phosphor. In general, TLDs have a precision of approximately 15% for low doses. This precision improves to approximately 3% for high doses (Berger and Hajek 2008).

I.E TLD Reader

A TLD reader system consists of a planchet for heating the TLD and a photomultiplier tube (PMT) for detecting the thermoluminescence light emission. The system converts light emitted from the TLD into an electrical signal which is linearly proportional to the detected photon fluence, then an electrometer records the signal as a charge or current. A schematic of a TLD reader is shown in Figure I.6.

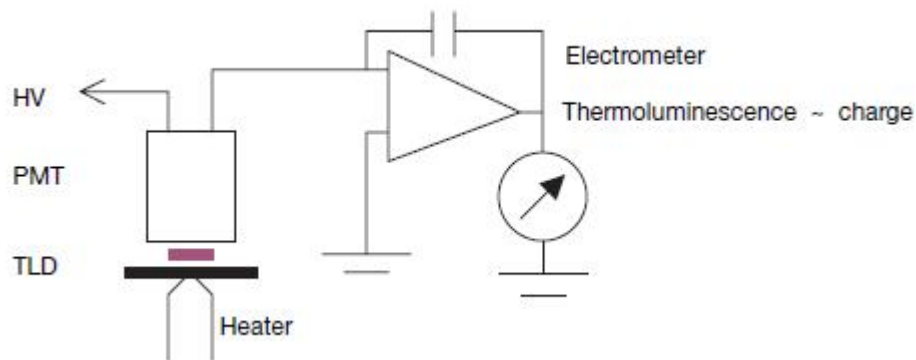


Figure I.6. Schematic of a basic TLD reader.

TLD glow curves can be generated from the TLD reader, which is the intensity of emitted light in terms of charge or current plot against the crystal temperature or time. The area under the curve is the total thermoluminescence signal emitted.

I.F Gamma Interactions in Matter

There are three common interactions when gamma photons interact with matter, namely, the Compton Effect, Photoelectric Effect and Pair Production (Attix 2004). The relative importance of the three interactions is summarized in Figure I.7, which illustrates the regions in which each interaction is dominant.

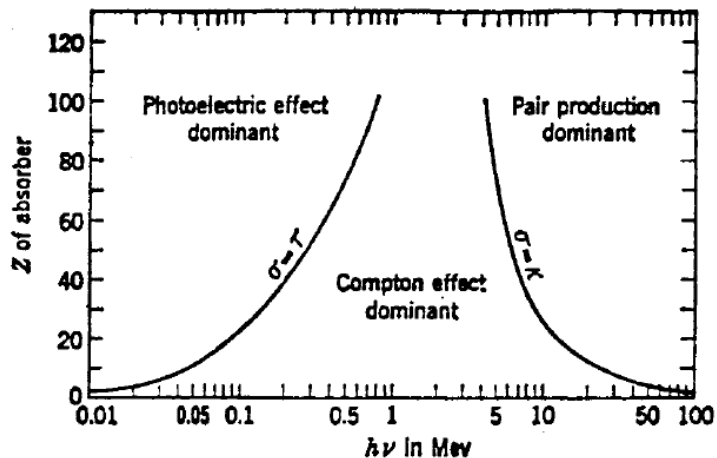


Figure I.7. Relative importance of the three common gamma interaction types (Attix 2004).

The photoelectric effect is the process of ejection of an electron when an atom absorbs energy from a gamma ray. The photon disappears in the process; some of its

energy overcomes the electron binding energy and the remainder is transferred to the freed electron as kinetic energy. The newly freed electron is called a photoelectron.

The Compton Effect is a form of inelastic scattering, in which a gamma ray interacts with a free or weakly bound electron and transfers part of its energy to the electron. The results of the Compton Effect include energy decrease of the gamma ray and the ejection of the electron by the atom, where the newly freed electron has kinetic energy essentially equal to the energy lost by the gamma ray. The Compton Effect is the dominant interaction in this research.

Pair Production is the creation of an electron and a positron pair. A gamma ray with an energy at least 1.022 MeV can create an electron-positron pair when it is under the influence of the strong electromagnetic field in the vicinity of a nucleus. If the gamma-ray energy exceeds 1.022 MeV, the excess energy is shared between the electron and the positron as kinetic energy. Although the threshold for this interaction is 1.022 MeV, the interaction has a low probability for photons below about 4 MeV (Oldenberg and Rasmussen 1996).

I.G X-Ray Beam Quality Specification

TLD chips must be annealed and calibrated before use. For TLD-700s, filtered x-rays are commonly used for calibration. The quality of an X-ray is usually specified in terms of its attenuation characteristics in a reference medium (commonly in Cu and Al) (Attix 2004), such as first and second half-value layers (HVL_1 , HVL_2), homogeneity coefficient (HC) and equivalent photon energy ($h\nu_{eq}$). HVL_1 is defined as the thickness

required to reduce the X-ray exposure by half in narrow-beam geometry. HVL_2 is the thickness necessary to reduce it by half again under the same conditions. The ratio HVL_1/HVL_2 is the homogeneity coefficient, which approaches unity as the spectrum is narrowed by filtration to approach monochromaticity. Lastly, $h\nu_{eq}$ is defined as the quantum energy of a monoenergetic beam having the same HVL_1 as the beam being specified.

I.H Relative Error

In statistics, relative error is generally expressed as a percentage to reflect how a quantity varies from the actual value. To obtain the relative error for a set of numbers, one must first identify the variance or the standard deviation of the set. Equation 3, 4 and 5 can be used to derive variance, standard deviation and relative error, respectively.

$$s^2 = \frac{1}{N-1} * \sum_i (x_i - \bar{X})^2 \quad (3)$$

$$s = \sqrt{s^2} \quad (4)$$

$$\text{relative error} = \frac{s}{\bar{X}} \quad (5)$$

where, s^2 is sample variance, N is sample size, x_i is the value of index i , \bar{X} is mean, s is standard deviation (Rice 1995).

II. MODELS AND METHODS

II.A. Overall Design

The basic components of the low-dose irradiator include source and shielding materials. To achieve the desired dose rate in a given space, one can manipulate the thickness of shielding, the distance between source and the target, the strength of the source or any combination of the three. However, for practical viability, this research chooses to use a pre-manufactured incubator, specifically, the Thermo Scientific Forma Series II Water Jacketed CO₂ Incubator, to act as shielding and simulate the space shuttle's exterior. Due to this design choice, one can only modify the two remaining factors, namely, the distance and the source strength to attain the desired dose rate.

The diagram of the irradiation system and the actual experiment setup are shown in Figure II.1 and II.2, respectively, where a bacteria culture vessel (target) is placed inside the incubator (shielding), which is surrounded by three, unit-length cobalt-60 wires.

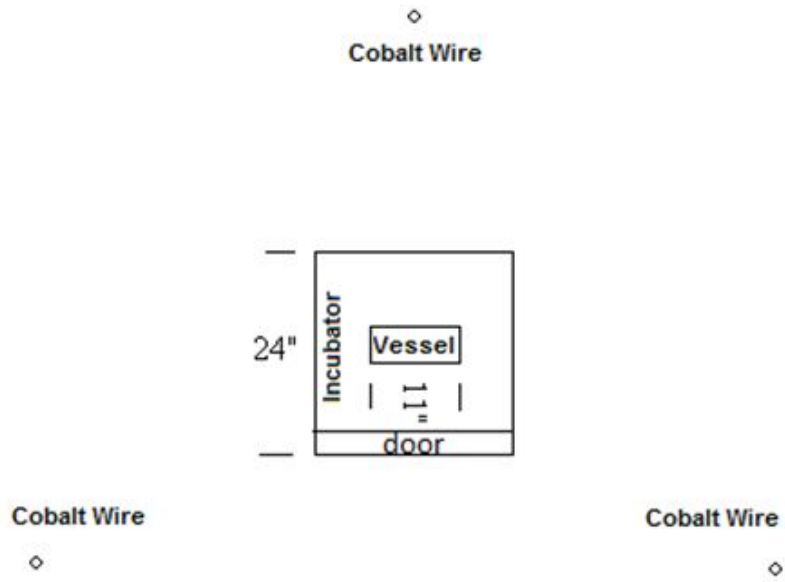


Figure II.1: Top view of irradiation system.



Figure II.2: Photo of the actual experiment setup.

II.B. Source

Radiation field strength directly depends on source activity. More specifically, the activity of each cobalt wire is required to compute the dose rate within the target. The cobalt wire of our choice (manufacturer Alfa Aesar, stock No. 10947, Lot No B23R004) has an exact diameter (0.25 mm) and length (1 m). Such a geometry can be used to calculate the volume of each wire using Equation 6,

$$V = \pi * r^2 * h \quad (6)$$

where V , r , h refer to volume, radius, and height, respectively.

Once the wire volume is determined, its mass can be calculated using Equation 7,

$$m = \rho * V \quad (7)$$

where, m is mass and ρ is density.

Consequently, the number of molecules can be calculated by using Equation 8,

$$N = \frac{m}{M} * Na \quad (8)$$

where, N is the number of molecules in the given mass, M is molar mass, and Na is Avogadro's constant.

Finally, the activity of each wire can be calculated by using Equations 9 and 10,

$$\lambda = \frac{\ln(2)}{T_{1/2}} \quad (9)$$

$$A = \lambda * N \quad (10)$$

where, A refers to activity of a 100% pure cobalt-60 wire, λ refers to the decay constant of Co-60, and $T_{1/2}$ refers to its corresponding half life.

Complete calculation for the activity of each cobalt wire is shown in Appendix C.

Once the possible maximum activity is calculated, one can choose an appropriate activity lower than the maximum, which corresponds to the pre-determined target dose rate. This was done by manipulating the Co-60 purity level using MCNPX simulation. After the final Co-60 activity for each wire was determined, they were produced by neutron activation in the reactor at the Nuclear Science Center. A schematic of the $(n, \gamma) \text{Co}^{60}$ reaction is illustrated in figure II.3. Relevant neutron activation parameters can be found in Table II.1.

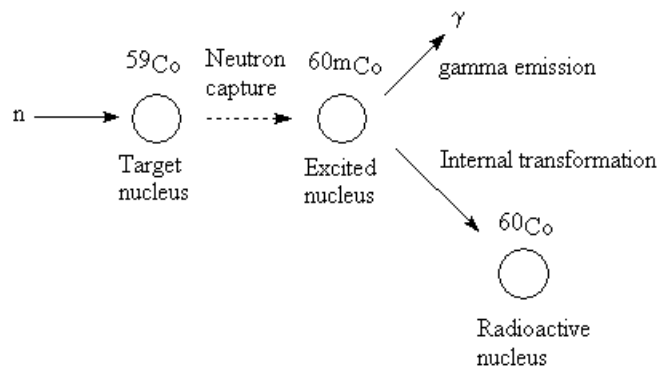


Figure II.3. Co-60 neutron activation schematic.

Table II.1. Neutron activation parameters for several materials (Beckurts and Wirtz 1964)

Element	Isotope (Abundance in Percent)	Thermal Activation Microscopic Cross Section (in 10^{-28} m^2)	Induced Activity	Half- Life
Manganese	^{55}Mn (100)	13.2 ± 0.1	^{56}Mn	2.58 h
Cobalt	^{59}Co (100)	16.9 ± 1.5	$^{60\text{m}}\text{Co}$	10.4 min
		20.2 ± 1.9	^{60}Co	5.28 y
Copper	^{63}Cu (69.1) ^{65}Cu (30.9)	4.41 ± 0.20	^{64}Cu	12.87 h
		1.8 ± 0.4	^{66}Cu	5.14 min
Silver	^{107}Ag (51.35) ^{109}Ag (48.65)	45 ± 4	^{108}Ag	2.3 min
		3.2 ± 0.4	$^{110\text{m}}\text{Ag}$	253 d
Indium	^{113}In (4.23)	56 ± 12	$^{114\text{m}_1}\text{In}$	49 d
		2.0 ± 0.6	^{114}In	72 s
	^{115}In (95.77)	160 ± 2 42 ± 1	$^{116\text{m}_1}\text{In}$ ^{116}In	54.12 min 14.1 s
Dysprosium	^{164}Dy (28.18)	2000 ± 200	$^{165\text{m}}\text{Dy}$	1.3 min
		800 ± 100	^{165}Dy	140 min
Gold	^{197}Au (100)	98.5 ± 0.4	^{198}Au	2.695 d

In theory, the initial activity of each wire can be calculated using in Equation 11.

$$A_0 = \frac{\sigma * m * \eta * \phi * \alpha * S}{w} \quad (11)$$

where,

A_0 = the activity of each wire at time of termination of neutron activation ($t=0$);

σ = neutron absorption cross section;

m = the mass of each wire in grams;

η = Avogadro's constant, $6.023 * 10^{23}$ molecules/mole;

ϕ = neutron fluence rate, neutrons/cm²/s;

α = fraction of target isotope in the sample, was 1 in this research, since Co^{59} is 100% abundant;

S = saturation factor, $1 - e^{-\lambda t}$; and

w = the atomic weight of element.

However, in practice, the wires had to be compressed into coils and placed inside aluminum capsules during activation, hence, one must account for the self-shielding and attenuation effects. Additionally, neutron fluence rate around the cobalt wire coils could not be guaranteed as constant for the entire activation duration.

Three wires were separately activated at reactor core position A4, using the reactor in Nuclear Science Center of Texas A&M University. The initial activity of the wires was estimated to be between 20 to 25 mCi. More detailed neutron activation records from Nuclear Science Center are shown in Appendix D.

As soon as the neutron activation process was terminated (t_0), the initial activity of cobalt wire (A_0) decreases over time due to radioactive decay. As shown in Figure II.4, the measured activity (counts) is proportional to the area under decay curve between the start time of measurement (t_1) and the end time of measurement (t_2). However, since Co-60 has a long half life of 5.28 years (Beckurts and Wirtz 1964) compared to the experiment duration of 30 days, one can treat the activity of cobalt wire as a constant for practical purposes throughout the experiment duration.

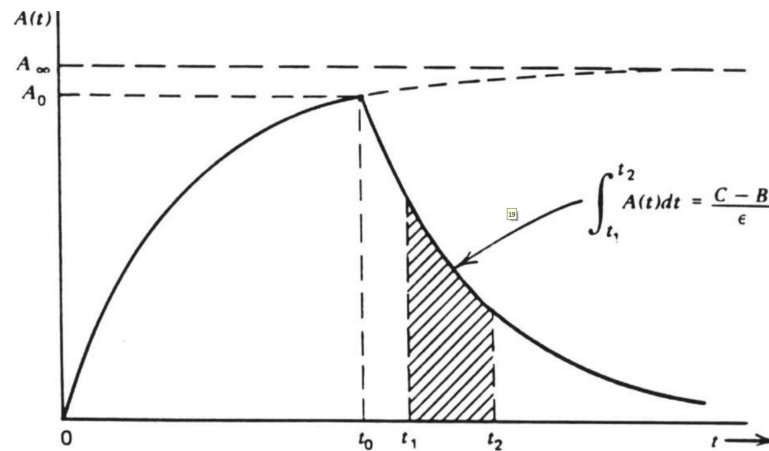


Figure II.4. The activity of an activator detector with respect to time. Where C is counts recorded between time t_1 and t_2 , B is background counts, ϵ is detector efficiency.

II.C. Shielding

As stated previously, a Thermo Scientific Forma Series II Water Jacketed CO₂ Incubator was used as shielding. The incubator wall has three layers of different materials: a 0.02 cm layer of stainless steel on the interior, a 3.65 cm thick water jacket is located between the interior and exterior walls, and finally a 2.3 cm layer of fiberglass (SiO₂) acts as the exterior wall. A picture of Thermo Scientific Forma Series II Water Jacketed CO₂ Incubator is shown in Figure II.5, and the specifications provided by the manufacturer are shown in Table II.2.

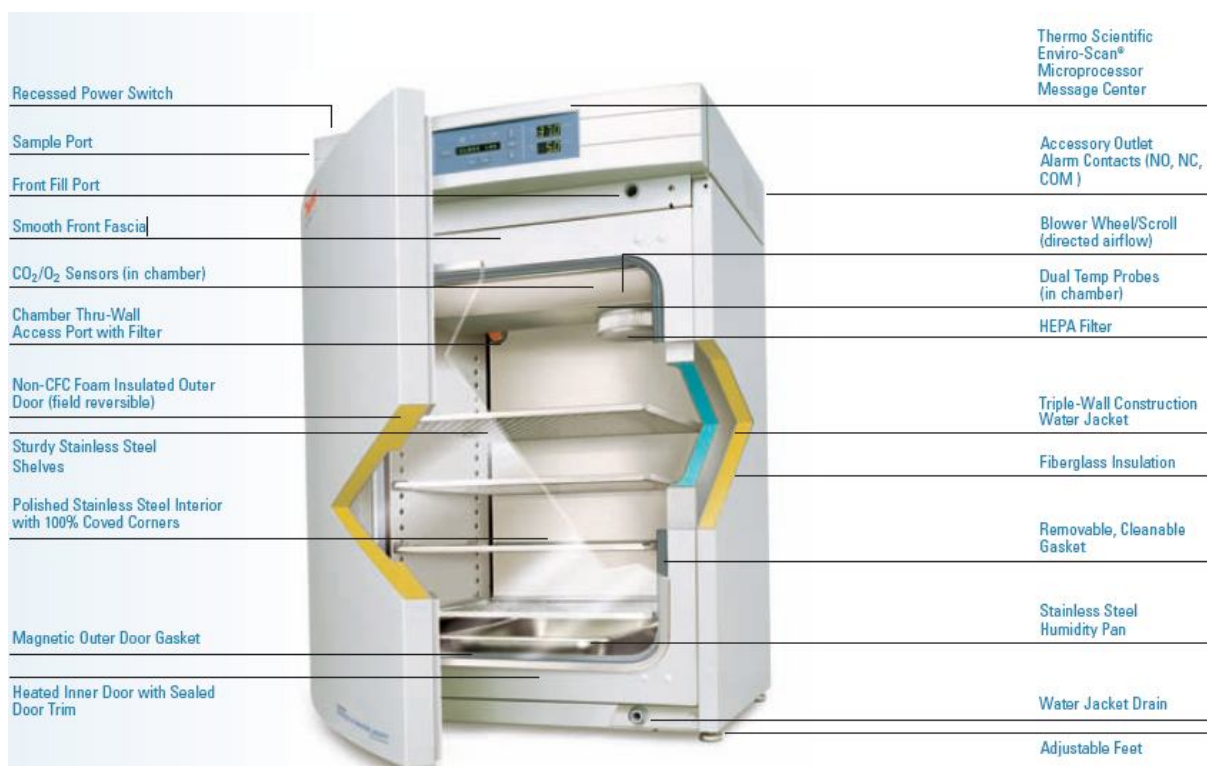


Figure II.5: Thermo Scientific Forma Series II Water Jacketed CO₂ Incubator (Thermo Scientific 2011).

Table II.2. Specifications of Thermo Scientific Forma Series II Water Jacketed CO₂ Incubator (Thermo Scientific 2011)

Specifications	
Capacity	6.5 cu. ft. (184 L)
Relative Humidity	Ambient to 95% at 37°C
Humidity System	3 L stainless-steel pan
Temperature Uniformity	±0.2°C at 37°C
Chamber	Polished stainless-steel interior with coved corners
Interior D x W x H	20.0 x 21.3 x 26.8 in. (50.8 x 54.1 x 68.1cm)
Shelving	Stainless steel
Exterior L x W x H	25 x 26.0 x 39.5 in. (63.5 x 66.0 x 110.3cm)
Net Weight	265 lb. (120.2kg)

For radiation shielding purposes, the most relevant information are the material compositions and thicknesses of the walls. Figure II.5 can be simplified by removing unnecessary physical features, such as racks and tubes, while retaining dimensions and material composition. This simplification can vastly decrease the computational time in MCNPX. The simplified diagram is shown in Figure II.6 (with bacteria culture vessel installed).

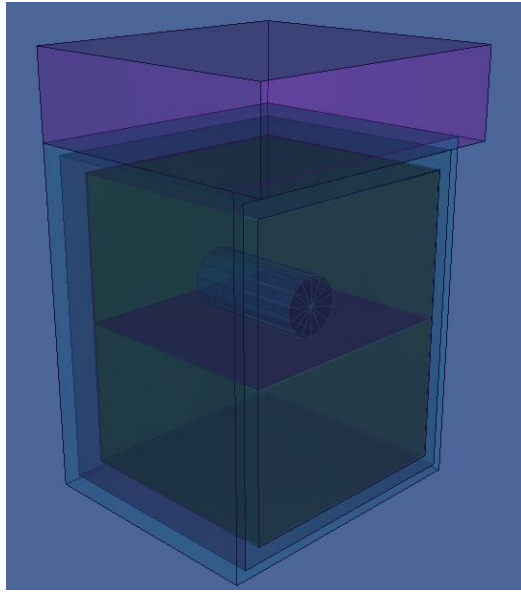


Figure II.6: Simplified incubator diagram with bacteria culture vessel.

II.D. Distance

Once the maximum source activity and the shielding materials are determined, the distance required to achieve a required dose rate can be obtained using MCNPX. For this research project, the method of choice is trial and error, also known as generate and test. To do this, a randomly selected distance and source activity, calculated by methods described in previous sections, along with shielding geometry are input into the MCNPX code to generate the dose rate inside the forged bacteria culture vessel. Since the target dose rate is inversely proportional to the square of the distance and proportional to source activity, one must increase the distance or decrease source activity or a combination of the two, if the calculated dose rate is higher than the planned dose rate, or vice versa. The appropriate combinations of distance and source activity for the planned bacterial vessel dose rate can be determined using methods described above. For

any given shielding geometry, there can be infinite numbers of distance and source activity combinations. However, the laboratory room used to perform the experiment could not accommodate distances greater than two meters. Due to this space constrain, the most realistic combination was 1 meter distance and 23 mCi activity for each cobalt wire. The geometry displayed in Figure II.6 was used in the MCNPX code that is found in Appendix A.

III. MEASUREMENTS AND SIMULATION

III.A. TLD

Fifteen TLDs were placed inside the incubator to map the radiation field. The incubator interior space was divided into two equal halves by a single stainless steel rack, on which the bacterial vessel rested. One group of four TLDs (numbers 1-4) were attached to the upper corners. Similarly, another two groups were attached to the middle (numbers 5-8) and lower corners (number 9-12), respectively. Finally, the last three TLDs (numbers 13-15) were placed within the bacterial vessel space on cylindrical axis. Their positions are illustrated in figure III.1.

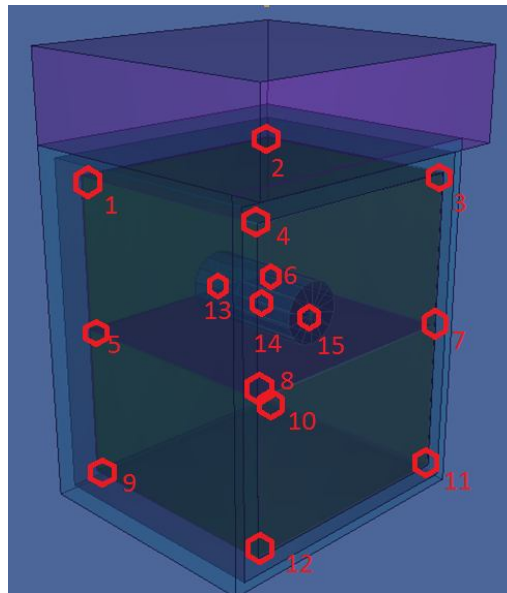


Figure III.1: TLD locations within the incubator.

Before the experiment, all TLDs were calibrated by using copper-filtered 250 kVp X-rays. To determine the equivalent photon energy of the filtered beam, two different thicknesses of aluminum were added to the copper layer, and exposure was recorded for each added layer. Table III.1 summarizes the copper and aluminum thickness and their corresponding exposures.

Table III.1. Calibration filtration metal thicknesses and exposures

Thickness of Cu (mm)	Thickness of Al (mm)	Exposure (R)	Relative Exposure
2.11	0	26.6	1
2.11	16.4	14.7	0.552
2.11	21.73	11.4	0.429

Equation 12 can be obtained by plotting aluminum thickness versus relative exposure in Excel with trendline function:

$$y = -0.0265 * x + 0.9976 \quad (12)$$

where, x is the thickness in millimeters and y is the relative exposure.

Hence, HVL_1 in aluminum can be obtained by setting y equals to 0.5 and solving for x in Equation 12. HVL_1 was calculated to be 18.78 mm; subsequently, the equivalent photon energy of the calibration X-ray was determined to be 160 keV by examining the Al curve in Figure III.2.

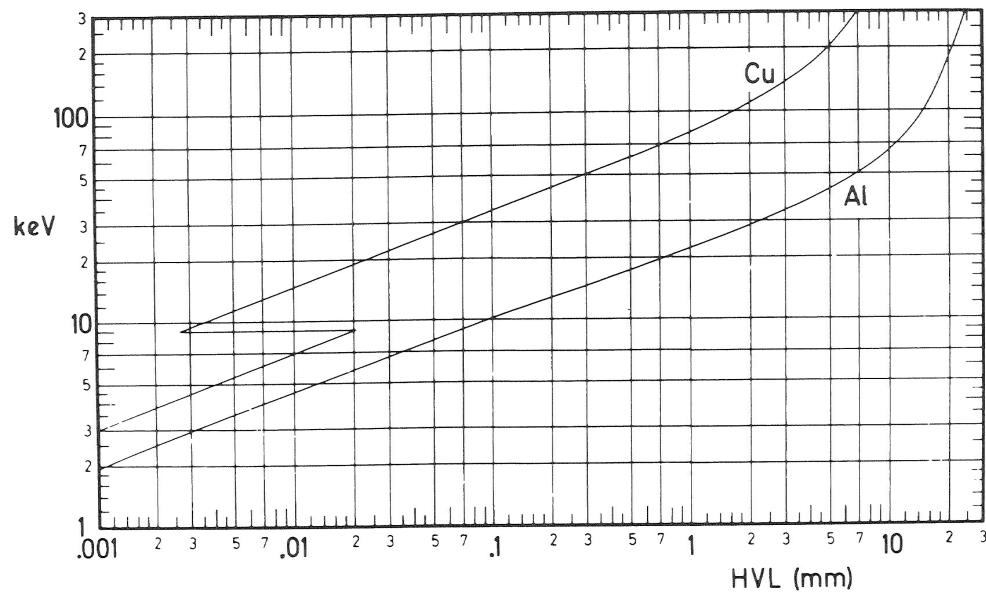


Figure III.2. Equivalent photon energy vs. HVL_1 in copper or aluminum. (Attix 2004).

Lithium fluoride TLDs typically show variations in efficiency for different energy ranges. Such trends can be visualized in Figure III.3, which summarizes the TLD response relative for photon energy from 6 to 2800 keV.

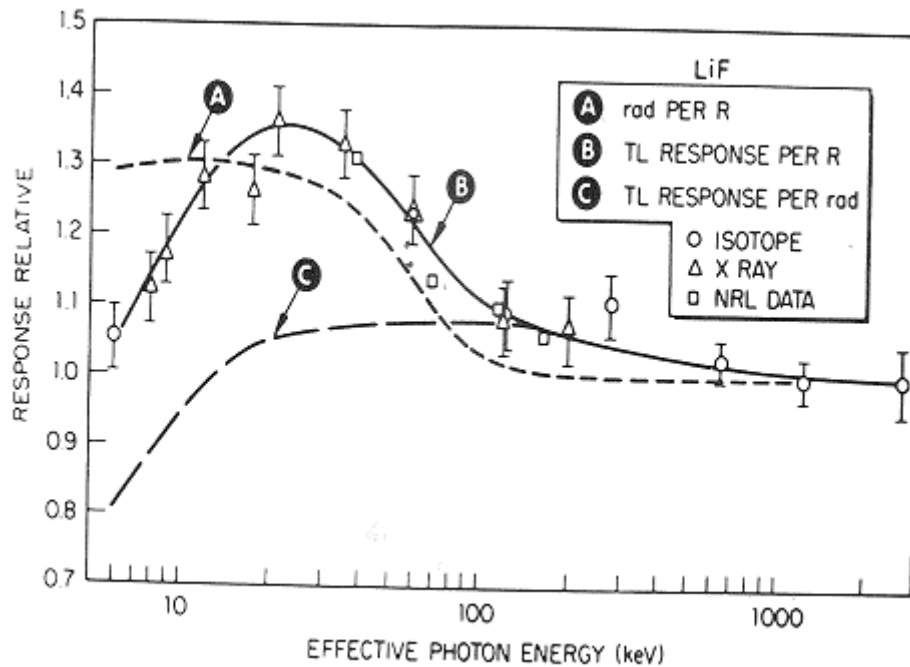


Figure III.3: Thermoluminescent response of LiF for photon energy from 6 to 2800 keV (Attix 2004).

As shown in Figure III.3, Curves A (rad per R) converges to 1 when photon energy is between 140 keV and 2800 keV. Since the calibration X-ray (160 keV equivalent) and gamma rays emitted from Co-60 (1173.2 keV and 1332.5 keV) lie within this energy range, the relative response coefficient is determined to be 1 for both calibration and measurement.

The fifteen TLDs were calibrated in two separate exposures (0.786 R and 1.086 R) using X-rays with an equivalent photon energy of 160 keV. The calibration results are shown in Table III.2.

Table III.2. TLD Calibration results after exposure to 0.786 and 1.086 R X-ray with equivalent photon energy of 160 keV

	0.786 R	1.086 R	0.786 R	1.086 R	Average
TLD Number	nC	nC	R/nC	R/nC	R/nC
1	69.503	70.439	0.011	0.015	0.013
2	76.471	78.060	0.010	0.014	0.012
3	138.311	81.506	0.006	0.013	0.010
4	155.390	77.182	0.005	0.014	0.010
5	77.645	81.224	0.010	0.013	0.012
6	70.431	96.154	0.011	0.011	0.011
7	62.562	53.368	0.013	0.020	0.016
8	50.077	59.276	0.016	0.018	0.017
9	71.778	78.165	0.011	0.014	0.012
10	48.949	61.703	0.016	0.018	0.017
11	89.655	82.768	0.009	0.013	0.011
12	73.571	68.460	0.011	0.016	0.013
13	65.637	75.735	0.012	0.014	0.013
14	62.697	64.288	0.013	0.017	0.015
15	90.726	75.560	0.009	0.014	0.012
Average	80.227	73.592			

Based on data from Table III.2, TLDs were observed to record higher averaged dose at lower X ray exposure. TLD #3 and #4 were thought to be the main contributors to this error. Examination on glow curves confirmed this suspicion. All calibration glow curves generated from 0.786 R and 1.086 R X-rays can be found in Appendix E and F, respectively.

Comparison between a typical glow curve, such TLD #1 after exposure to 0.786 R X-ray (Fig III.4) and disputed glow curves of TLD #3 (0.786 R) (Fig III.5) and #4 (0.786 R) (Fig III.6) revealed that main dosimetric peak was single peak for TLD #1, however, it was double peaks for #3 and #4. This error was most likely due to uneven heating in the TLD reader's planchet during reading, a common cause for TLD reader

inaccuracy. Because thermoluminescence intensity emission is a function of the TLD temperature (T), keeping the heating rate constant makes the temperature proportional to time (channel), and so the thermoluminescence intensity can be plotted as a function of time. However, if the heating rate is not constant, the above statement cannot hold true, resulting signal shift with respect to time (channel). In cases of TLD #3 and #4, light emitted around channel 60 was shifted to the left, which then compounded with the main dosimetric peak, therefore, produced a larger area under the glow curve.

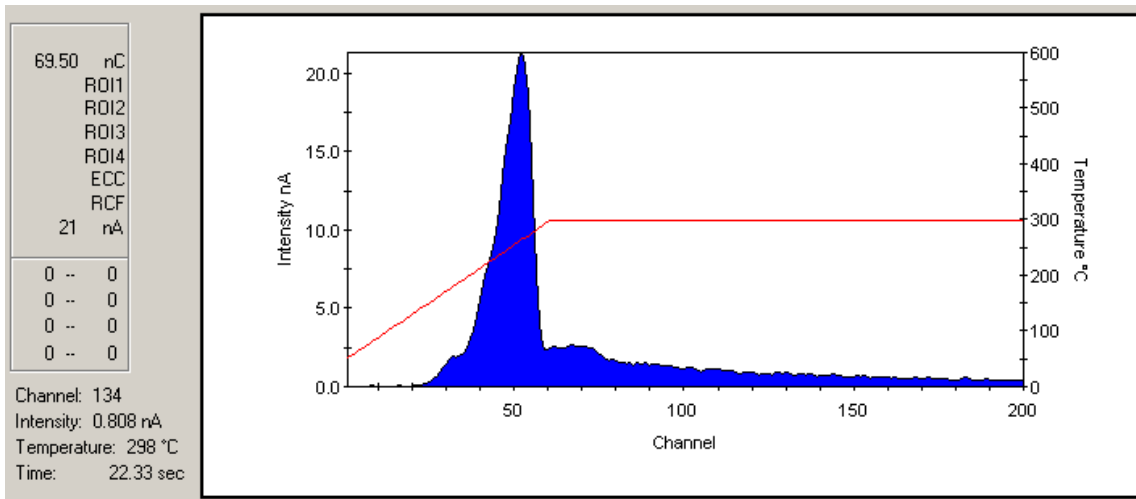


Figure III.4: Glow curve of TLD #1 after exposure to 0.786 R X-ray.

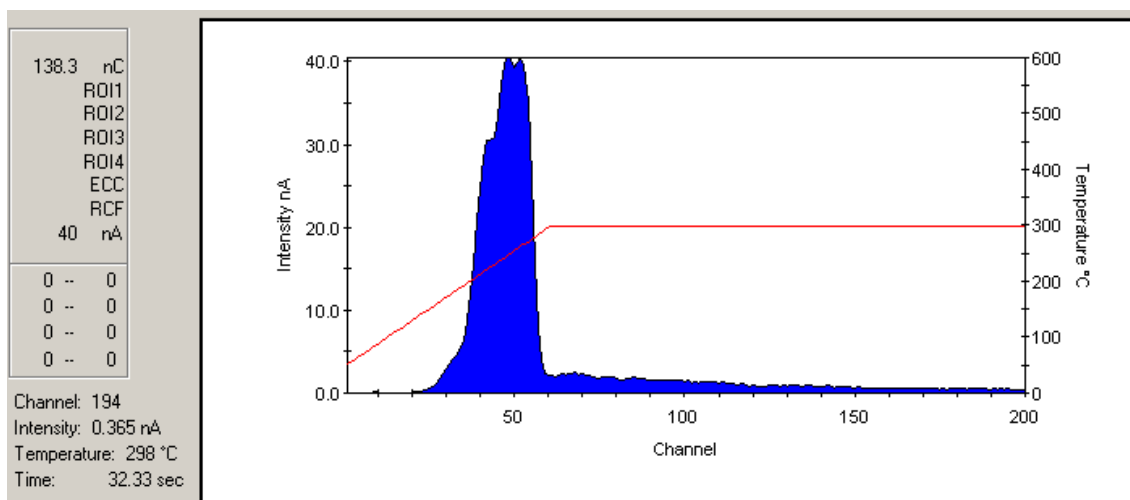


Figure III.5: Glow curve of TLD #3 after exposure to 0.786 R X-ray. Because signal around channel 60 was shifted to channel 50 where the main dosimetric peak was located, the compounded signal resulted double peaks and larger area under the curve.

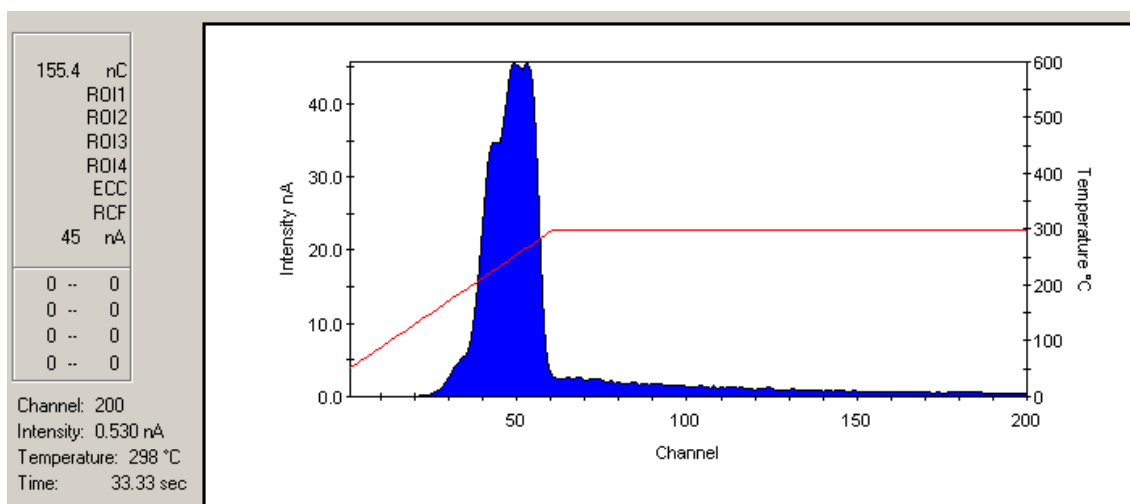


Figure III.6: Glow curve of TLD #4 after exposure to 0.786 R X-ray.

Due to reason stated above, dose resulted from 0.786 R X-ray in TLD #3 and #4 were excluded from calibration. Modified calibration summary is shown in Table III.3.

Table III.3. Modified TLD calibration results

	0.786 R	1.086 R	0.786 R	1.086 R	Average
TLD Number	nC	nC	R/nC	R/nC	R/nC
1	69.503	70.439	0.011	0.015	0.013
2	76.471	78.060	0.010	0.014	0.012
3	Excluded	81.506	Excluded	0.013	0.013
4	Excluded	77.182	Excluded	0.014	0.014
5	77.645	81.224	0.010	0.013	0.012
6	70.431	96.154	0.011	0.011	0.011
7	62.562	53.368	0.013	0.020	0.016
8	50.077	59.276	0.016	0.018	0.017
9	71.778	78.165	0.011	0.014	0.012
10	48.949	61.703	0.016	0.018	0.017
11	89.655	82.768	0.009	0.013	0.011
12	73.571	68.460	0.011	0.016	0.013
13	65.637	75.735	0.012	0.014	0.013
14	62.697	64.288	0.013	0.017	0.015
15	90.726	75.560	0.009	0.014	0.012
Average	69.977	73.593			

Once calibrated, the TLDs were placed inside the incubator to map the radiation field. During a period of thirty days, seven sets of measurements were performed, and each measurement lasted eight hours. The measurement results are shown in Table III.4, and their glow curves are shown in Appendix G.

Table III.4. Results of seven different exposures measured in nanocoulombs (nC)

TLD	Exposure (nC)							
	1	2	3	4	5	6	7	Average
1	30.266	36.922	40.061	44.985	42.549	43.974	36.940	39.385
2	28.324	36.261	36.458	37.929	51.090	35.040	39.025	37.732
3	28.293	32.424	35.140	35.678	32.036	30.903	26.341	31.545
4	35.695	38.666	39.211	31.839	32.099	30.690	32.503	34.386
5	34.432	35.622	36.234	34.981	32.001	34.126	40.233	35.376
6	41.909	41.197	43.829	45.046	42.275	54.519	33.804	43.226
7	23.915	29.266	31.337	28.303	26.346	28.810	19.903	26.840
8	25.812	27.858	31.780	26.331	25.827	27.356	27.265	27.461
9	27.244	32.325	35.968	30.157	29.515	39.922	33.583	32.673
10	29.654	64.272	46.866	45.499	27.918	31.512	30.296	39.431
11	33.685	44.726	61.814	33.874	28.220	34.467	35.712	38.928
12	24.736	34.329	27.306	29.573	25.570	24.301	25.965	27.397
13	34.232	31.814	31.192	37.251	38.716	27.626	22.147	31.854
14	32.495	33.709	43.723	29.650	22.633	34.701	25.272	31.740
15	27.878	34.153	33.583	37.223	28.011	31.247	29.468	31.652

The original TLD exposures were measured in nanocoulombs (nC), however, using calibration factors from Table III.3, one can convert the free-space exposure (X) unit from nanocoulomb (nC) to roentgen (R). The converted exposure is summarized in Table III.5.

Table III.5. Results of seven different exposures measured in roentgens (R)

TLD	Exposure (R)							Average
	1	2	3	4	5	6	7	
1	0.393	0.480	0.521	0.585	0.553	0.572	0.480	0.512
2	0.340	0.435	0.437	0.455	0.613	0.420	0.468	0.453
3	0.368	0.422	0.457	0.464	0.416	0.402	0.342	0.410
4	0.500	0.541	0.549	0.446	0.449	0.430	0.455	0.481
5	0.413	0.427	0.435	0.420	0.384	0.410	0.483	0.425
6	0.461	0.453	0.482	0.496	0.465	0.600	0.372	0.475
7	0.383	0.468	0.501	0.453	0.422	0.461	0.318	0.429
8	0.439	0.474	0.540	0.448	0.439	0.465	0.464	0.467
9	0.327	0.388	0.432	0.362	0.354	0.479	0.403	0.392
10	0.504	1.093	0.797	0.773	0.475	0.536	0.515	0.670
11	0.371	0.492	0.680	0.373	0.310	0.379	0.393	0.428
12	0.322	0.446	0.355	0.384	0.332	0.316	0.338	0.356
13	0.445	0.414	0.405	0.484	0.503	0.359	0.288	0.414
14	0.487	0.506	0.656	0.445	0.339	0.521	0.379	0.476
15	0.335	0.410	0.403	0.447	0.336	0.375	0.354	0.380

To obtain the absorbed dose (D_a) from these exposures (X), one must change the exposure unit from roentgen (R) to coulomb per kilogram (C/kg) by using Equation 13 before relating exposure to dose by Equation 14,

$$1 \text{ R} = 2.58\text{E-}4 \text{ C/kg} \quad (13)$$

$$D_a = X * \left(\frac{\overline{W}}{e} \right)_a \quad (14)$$

where D_a is absorbed dose in Gy, X is the exposure in C/kg, and $(\overline{W}/e)_a$ is the mean energy per unit charge released, having the value 33.97 J/C in air under room condition.

The absorbed dose derived by above method is summarized in Table III.6.

Table III.6. Absorbed dose of seven TLD exposures

TLD	Absorbed Dose (Gy)							
	1	2	3	4	5	6	7	Average
1	3.45E-03	4.21E-03	4.56E-03	5.13E-03	4.85E-03	5.01E-03	4.21E-03	4.49E-03
2	2.98E-03	3.81E-03	3.83E-03	3.99E-03	5.37E-03	3.69E-03	4.10E-03	3.97E-03
3	3.22E-03	3.69E-03	4.00E-03	4.06E-03	3.65E-03	3.52E-03	3.00E-03	3.59E-03
4	4.38E-03	4.74E-03	4.81E-03	3.91E-03	3.94E-03	3.77E-03	3.99E-03	4.22E-03
5	3.62E-03	3.75E-03	3.81E-03	3.68E-03	3.37E-03	3.59E-03	4.23E-03	3.72E-03
6	4.04E-03	3.97E-03	4.23E-03	4.34E-03	4.08E-03	5.26E-03	3.26E-03	4.17E-03
7	3.35E-03	4.10E-03	4.39E-03	3.97E-03	3.69E-03	4.04E-03	2.79E-03	3.76E-03
8	3.85E-03	4.15E-03	4.73E-03	3.92E-03	3.85E-03	4.08E-03	4.06E-03	4.09E-03
9	2.87E-03	3.40E-03	3.78E-03	3.17E-03	3.10E-03	4.20E-03	3.53E-03	3.44E-03
10	4.42E-03	9.58E-03	6.98E-03	6.78E-03	4.16E-03	4.70E-03	4.51E-03	5.87E-03
11	3.25E-03	4.31E-03	5.96E-03	3.27E-03	2.72E-03	3.32E-03	3.44E-03	3.75E-03
12	2.82E-03	3.91E-03	3.11E-03	3.37E-03	2.91E-03	2.77E-03	2.96E-03	3.12E-03
13	3.90E-03	3.62E-03	3.55E-03	4.24E-03	4.41E-03	3.15E-03	2.52E-03	3.63E-03
14	4.27E-03	4.43E-03	5.75E-03	3.90E-03	2.98E-03	4.56E-03	3.32E-03	4.17E-03
15	2.93E-03	3.59E-03	3.53E-03	3.91E-03	2.95E-03	3.29E-03	3.10E-03	3.33E-03

Because the experiment location (beam port 4 on Lower Research Level at the Nuclear Science Center, TAMU) is near the vicinity of a nuclear reactor, one should consider the effects of background radiation from the reactor on TLD results. Based on a survey with a digital ion chamber (SN# 11332/2109), the experiment location had a background exposure rate of 42 mR/h when the reactor is operating at maximum power (1 MW), and a background exposure rate of 37 mR/h when the reactor is shutdown. Records from the reactor log showed that the reactor was operating at maximum power during the first five exposures; was shutdown during the sixth measurement; and was operating at low power during the seventh measurement. A more detailed summary of reactor operation is shown in Table III.7.

Table III.7. Summary of reactor operations from 6/14/10 to 7/12/10

Measurement #	Date	Rx Operating Power	Duration
1	6/14/2010	1 MW	all day
2	6/17/2010	1 MW	all day
3	6/22/2010	1 MW	all day
4	6/25/2010	1 MW	all day
5	6/30/2010	1 MW	all day
6	7/5/2010	Shutdown	shutdown all day
7	7/12/2010	100 W	2:26 pm - 5:08 pm

On 7/12/2010, the reactor was operating at low power (0.1% of maximum) and was only partially operating when the measurements were in progress. For this reason, the reactor can be considered shutdown for measurement #7. The background exposure rate difference between reactor operating and not operating is 5 mR/h (inside of the incubator). Using methods described earlier in this section, the background radiation from the reactor would result 3.50E-4 Gy in eight hours. The corrected eight hour absorbed dose of the fifteen TLDs is summarized in Table III.8.

Table III.8. Corrected absorbed dose of seven TLD exposures

TLD	Absorbed Dose (Gy)							Average
	1	2	3	4	5	6	7	
1	3.10E-03	3.86E-03	4.21E-03	4.78E-03	4.50E-03	5.01E-03	4.21E-03	4.24E-03
2	2.63E-03	3.46E-03	3.48E-03	3.64E-03	5.02E-03	3.69E-03	4.10E-03	3.72E-03
3	2.87E-03	3.34E-03	3.65E-03	3.71E-03	3.30E-03	3.52E-03	3.00E-03	3.34E-03
4	4.03E-03	4.39E-03	4.46E-03	3.56E-03	3.59E-03	3.77E-03	3.99E-03	3.97E-03
5	3.27E-03	3.40E-03	3.46E-03	3.33E-03	3.02E-03	3.59E-03	4.23E-03	3.47E-03
6	3.69E-03	3.62E-03	3.88E-03	3.99E-03	3.73E-03	5.26E-03	3.26E-03	3.92E-03
7	3.00E-03	3.75E-03	4.04E-03	3.62E-03	3.34E-03	4.04E-03	2.79E-03	3.51E-03
8	3.50E-03	3.80E-03	4.38E-03	3.57E-03	3.50E-03	4.08E-03	4.06E-03	3.84E-03
9	2.52E-03	3.05E-03	3.43E-03	2.82E-03	2.75E-03	4.20E-03	3.53E-03	3.19E-03
10	4.07E-03	9.23E-03	6.63E-03	6.43E-03	3.81E-03	4.70E-03	4.51E-03	5.62E-03
11	2.90E-03	3.96E-03	5.61E-03	2.92E-03	2.37E-03	3.32E-03	3.44E-03	3.50E-03
12	2.47E-03	3.56E-03	2.76E-03	3.02E-03	2.56E-03	2.77E-03	2.96E-03	2.87E-03
13	3.55E-03	3.27E-03	3.20E-03	3.89E-03	4.06E-03	3.15E-03	2.52E-03	3.38E-03
14	3.92E-03	4.08E-03	5.40E-03	3.55E-03	2.63E-03	4.56E-03	3.32E-03	3.92E-03
15	2.58E-03	3.24E-03	3.18E-03	3.56E-03	2.60E-03	3.29E-03	3.10E-03	3.08E-03

One can assume the background value is a constant; therefore, the variance of background is zero.

III.B. MCNPX Simulation

The computer code MCNPX was used to simulate the experiment. The computer generated geometries using Visual Editor are shown in Figure III.7 and III.8, where the red color represents the water, blue represents the fiberglass, and the purple represents the cobalt wires.

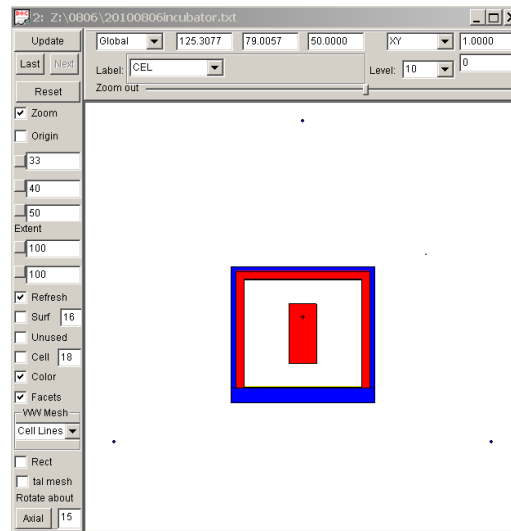


Figure III.7. XY cross section of the irradiation system.

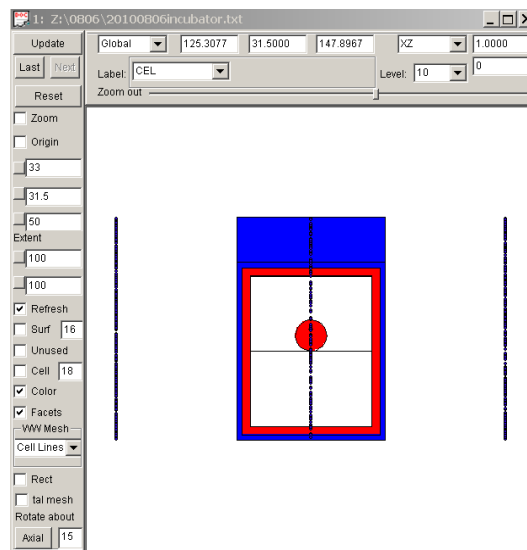


Figure III.8. XZ cross section of the irradiation system.

Figures III.9 and III.10 illustrate the material interaction and the tracks of gamma rays (green line). In each figure, only one thousand histories were used to prevent over display of photon paths. Photons that did not enter the incubator were simply ignored.

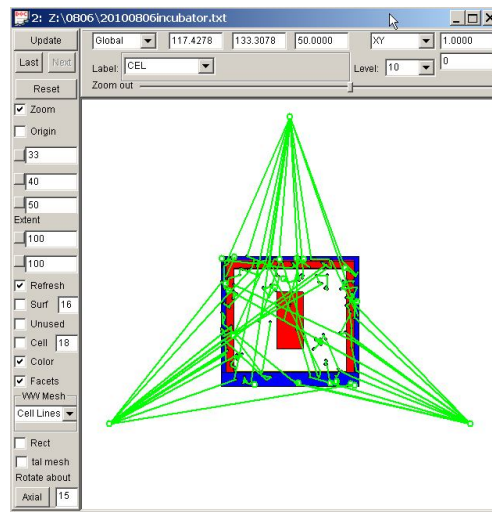


Figure III.9. XY cross section of the irradiation system with photon paths.

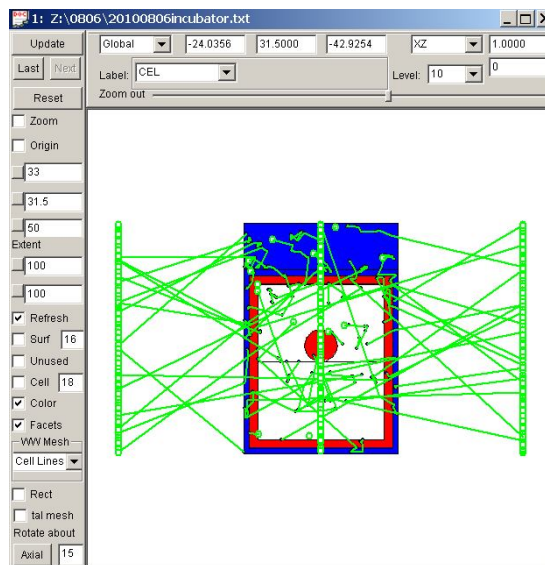


Figure III.10. XZ cross section of the irradiation system with photon paths.

Absorbed dose at any given location depends directly on the fluence (ϕ) at the location and particle energy (E). Using the MCNPX mesh tally, particle fluence distribution of any given plane within a defined volume can be differentiated by colors

(Guan, 2009). To visualize the fluence inside the incubator space, seven planes which contained various points of interest were chosen. Amongst them, four were horizontal planes at different elevations and three were vertical planes at different depths. One hundred million histories were used in the mesh tally to simulate the particle fluence.

Plane A (contained point # 1, 2, 3, 4), B (contained point # 5, 6, 7, 8), C (contained point # 9, 10, 11, 12) and D (contained point # 13, 14, 15) were horizontal planes. In terms of elevations, Plane A was the highest, positioned at the very top of incubator interior; Plane B was middle plane, dividing the interior space into two equal halves horizontally; Plane C was the lowest, positioned at the bottom of incubator interior; Plane D was positioned 2 cm above Plane B.

Plane E (contained points # 3, 4, 7, 8, 11, 12), F (contained point #14) and G (contained points # 1, 2, 5, 6, 9, 10) were vertical planes at different depths. Amongst them, Plane E was the front-most, positioned right behind the incubator door. Plane F was the middle plane. It divided the interior space into two equal halves vertically. Plane G was the farthest vertical plane away from the door, positioned right in front of the incubator back wall.

As shown in Figures III.11, III.12, III.13, III.14, all the horizontal planes had very similar gamma fluence distribution patterns, which the fluence distribution was homogenous for regions away from the door. For small areas near the incubator door, the fluence was significantly lower than the fluence further inside the incubator.

On the other hand, as shown in Figures III.15, III.16 and III.17, gamma fluence in vertical planes exhibited more random distribution patterns. For Plane E, the front vertical plane, gamma fluence was the highest near the left and right edges and was the lowest near the center. Within this plane, the fluence minimum was about 40% lower than the maximum. For Plane F, the middle plane, the gamma fluence was the highest near regions at 60 cm elevation and was the lowest near the top and bottom. Fluence minimum was about 25% lower than the maximum within Plane F. For Plane G, the back vertical plane, the gamma fluence was the highest near regions at 50 cm elevation and was the lowest near bottom. Fluence minimum was about 30% lower than the maximum within Plane G. Comparing all three vertical planes, the average fluence for the frontal vertical plane was the lowest and was the highest for the back vertical plane. The gamma fluence appeared to be increasing with increased depth, which agreed with the observation found in horizontal planes.

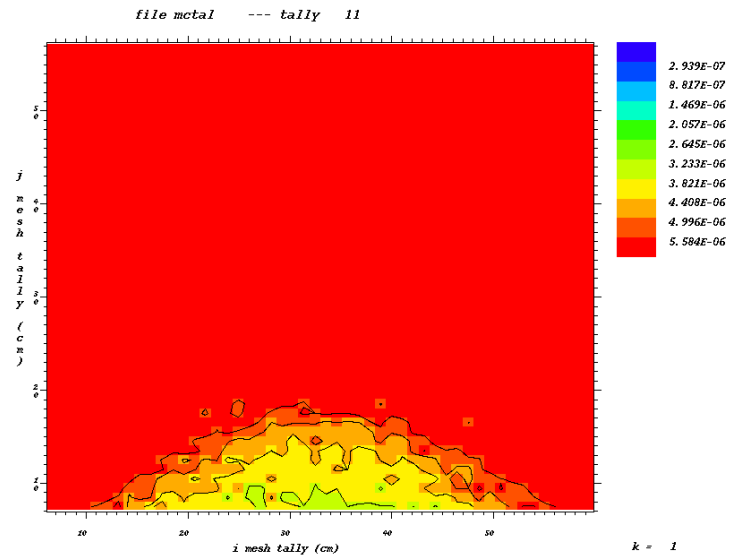


Figure III.11. Gamma fluence distribution in Plane A. This is a horizontal plane, which contained points # 1, 2, 3, 4. The distribution were mostly homogeneous, except a small area near the door, which was about 50% lower than the rear area. This distribution pattern was very similar to distribution observed in other horizontal planes.

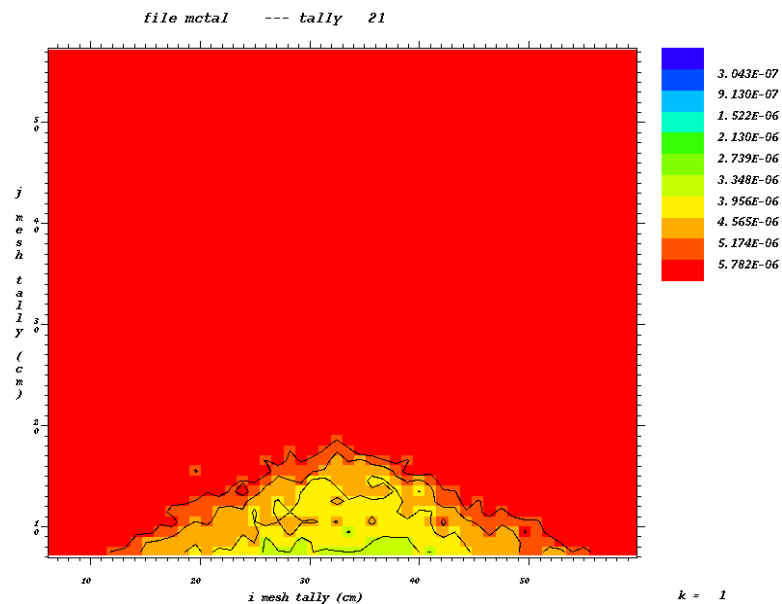


Figure III.12. Gamma fluence distribution in Plane B. This is a horizontal plane which contained points # 5, 6, 7, 8. This distribution pattern was very similar to distribution observed in other horizontal planes.

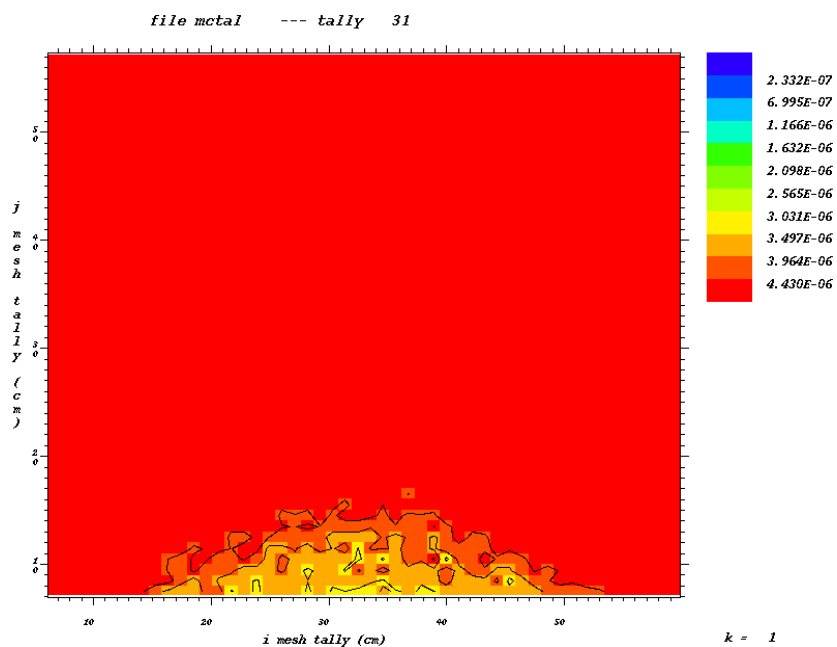


Figure III.13. Gamma fluence distribution in Plane C. This is a horizontal plane which contained points # 9, 10, 11, 12. This distribution pattern was very similar to distribution observed in other horizontal planes.

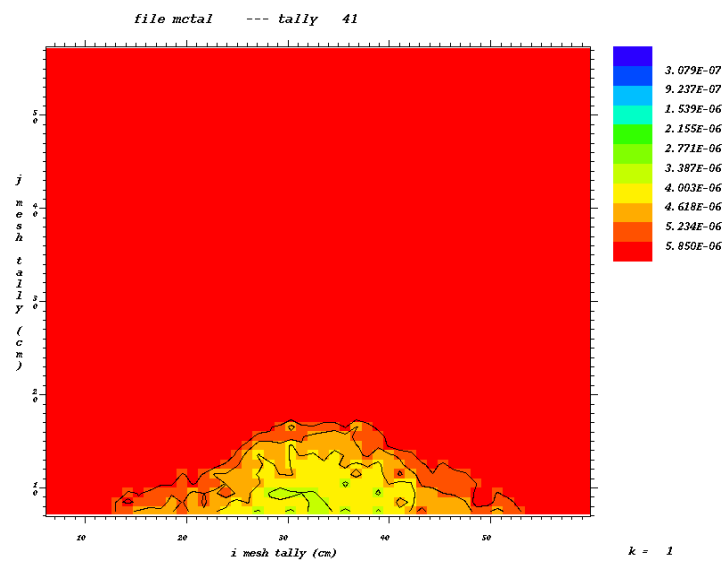


Figure III.14. Gamma fluence distribution in Plane D. This is a horizontal plane which contained points # 13, 14, 15. This distribution pattern was very similar to distribution observed in other horizontal planes.

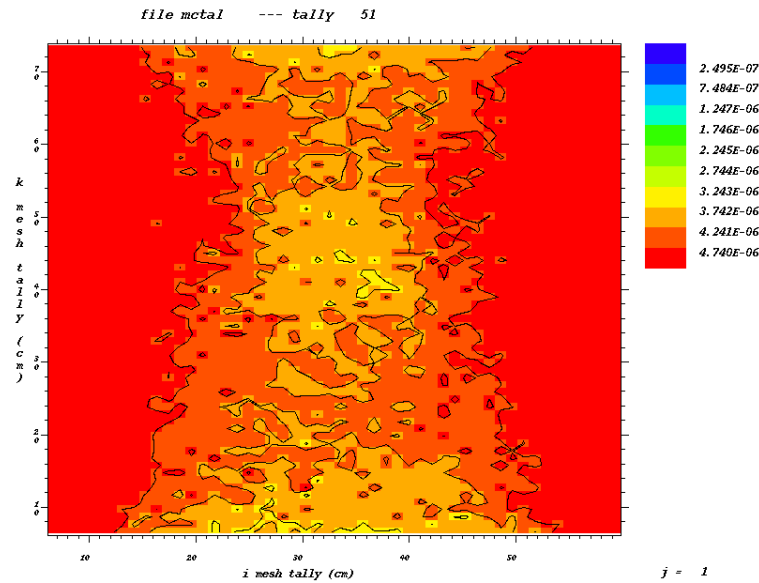


Figure III.15. Gamma fluence distribution in Plane E. This is a vertical plane which contained points # 3, 4, 7, 8, 11, 12. This figure shows the distribution just behind the incubator door, which fluence near the center was lower than fluence at left and right edges.

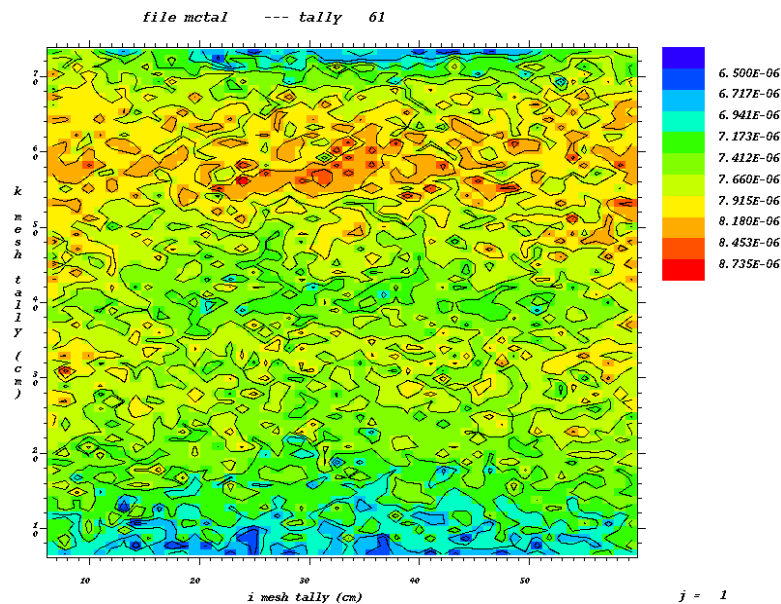


Figure III.16. Gamma fluence distribution in Plane F. This is a vertical plane which divides the incubator space into two equal halves. Gamma fluence is the lowest near the top and bottom and is the highest around 60 cm height. Gamma fluence in this figure is higher than Figure III.14 and lower than Figure III.15.

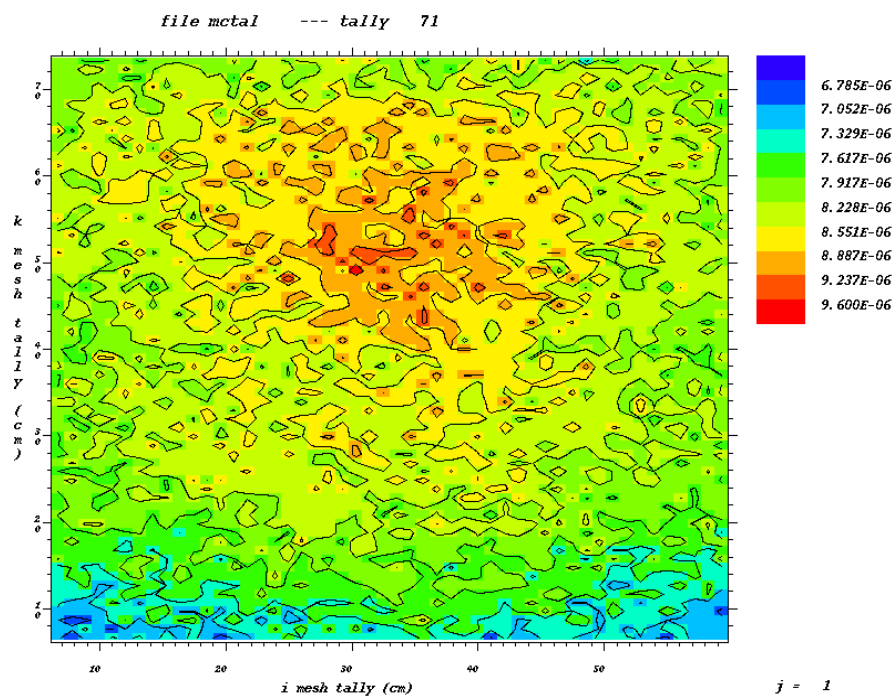


Figure III.17. Gamma fluence distribution in Plane G. This is a vertical plane which contained points # 1, 2, 5, 6, 9, 10. This plane is the farthest vertical plane away from the door within the incubator space. Gamma fluence was the lowest near the bottom and was highest around 50 cm height. Gamma fluence in this figure was higher than both Figure III.13 and III.14.

As illustrated in figures III.9 and III.10, gamma radiation interacts with the shielding materials before reaching the fifteen points of interest. Their interaction with matter along the particle tracks attenuates their initial energies of 1.1732 MeV and 1.3325 MeV (Mayo, 1998), resulting in a new spectrum of energies at the points of interest. The MCNPX F5 tally was used to obtain fluence at the points of interest (photons/ cm²). Subsequently, using fluence-to-dose conversion coefficients for air kerma per unit fluence (K_a/ϕ_a) for monoenergetic photons (ICRU 1992) shown in Table III.9, the MCNPX code can be used to calculate the absorbed dose from a single radiation for any point of interest. For the seven planes (plane A, B, C, D, E, F and G)

mentioned above, the distributions of averaged absorbed dose from a single source particle are shown in Figures III.18, III.19, III.20, III.21, III.22, III.23 and III.24.

As shown in Figures III.18, III.19 and III.20, the horizontal absorbed dose distributions in Plane A, B and C were similar to gamma fluence distributions in their respective planes, where absorbed dose was homogeneous in the rear area and gradually decreased towards the door area. For Plane D, in addition to the features observed in Planes A, B and C, a clear silhouette of the culture vessel's cross section can be seen due to the difference in absorbed dose. Figure III.21 suggested the absorbed dose within the culture vessel was uniform and was lower than the dose near the rear area but higher than dose near the door area.

Like the horizontal planes, the vertical plane absorbed dose distributions exhibited very close resemblance to their corresponding fluence counter parts. For Plane E, absorbed dose was the highest at the left and right edges and gradually decreased towards the center. For Plane F, where the plane intercepted the culture vessel volume, a clear circular silhouette was seen, indicating the difference in absorbed doses between the vessel and its surroundings. In this plane, the lowest absorbed dose was the area within the vessel, and the highest absorbed dose was the area just above the vessel. For Plane G, absorbed dose was the highest at 50 cm elevation and was the lowest at the bottom. Comparison of all three vertical planes suggested absorbed dose was the lowest near the door and gradually increased toward the rear area. This result matched the earlier horizontal observation.

Table III.9. Conversion coefficients for air kerma per unit fluence (K_a/ϕ_a) for monoenergetic photons (ICRU 1992)

Photon energy (MeV)	K_a/Φ (pGy cm ²)
0.010	7.430
0.015	3.120
0.020	1.680
0.030	0.721
0.040	0.429
0.050	0.323
0.060	0.289
0.080	0.307
0.100	0.371
0.150	0.599
0.200	0.856
0.300	1.380
0.400	1.890
0.500	2.380
0.600	2.840
0.800	3.690
1.000	4.470
1.500	6.140
2.000	7.550
3.000	9.960
4.000	12.100
5.000	14.100
6.000	16.100
8.000	20.100
10.000	24.000

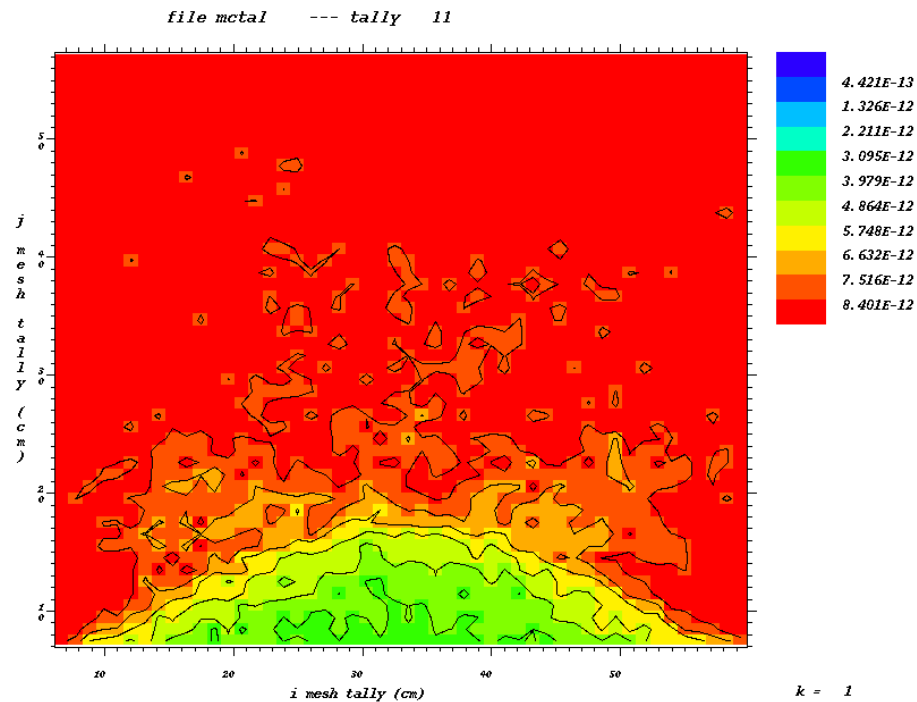


Figure III.18. Distribution of averaged absorbed dose from single source photon in Plane A. Similar to gamma fluence distribution, the averaged absorbed dose was more homogeneous in the rear. Additionally, dose near the incubator door was significantly lower than dose in the back. This distribution pattern was very similar to distribution observed in other horizontal planes.

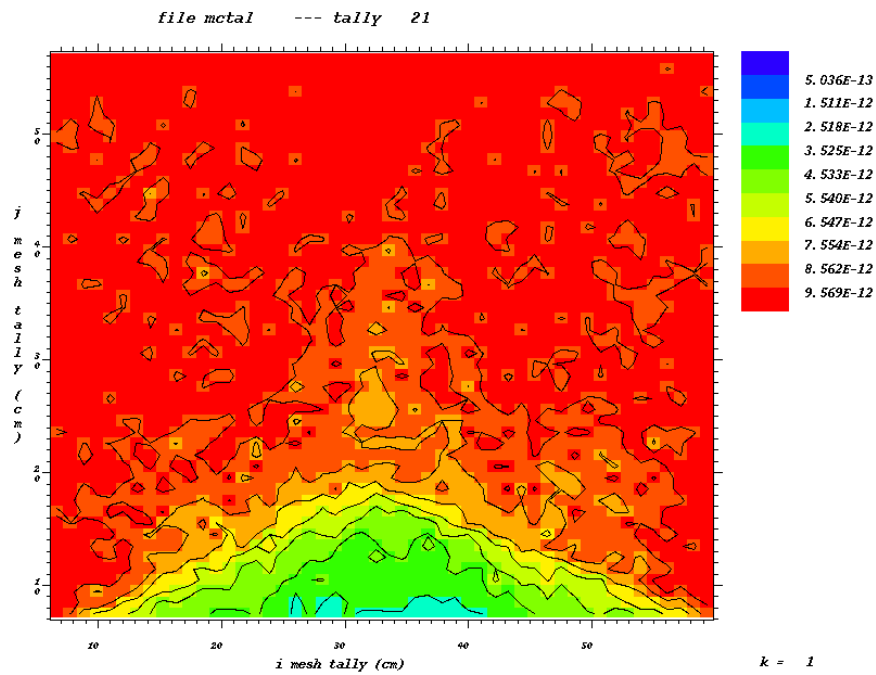


Figure III.19. Distribution of averaged absorbed dose from single source photon in Plane B. This dose distribution pattern was similar to distribution observed in Plane A and C.

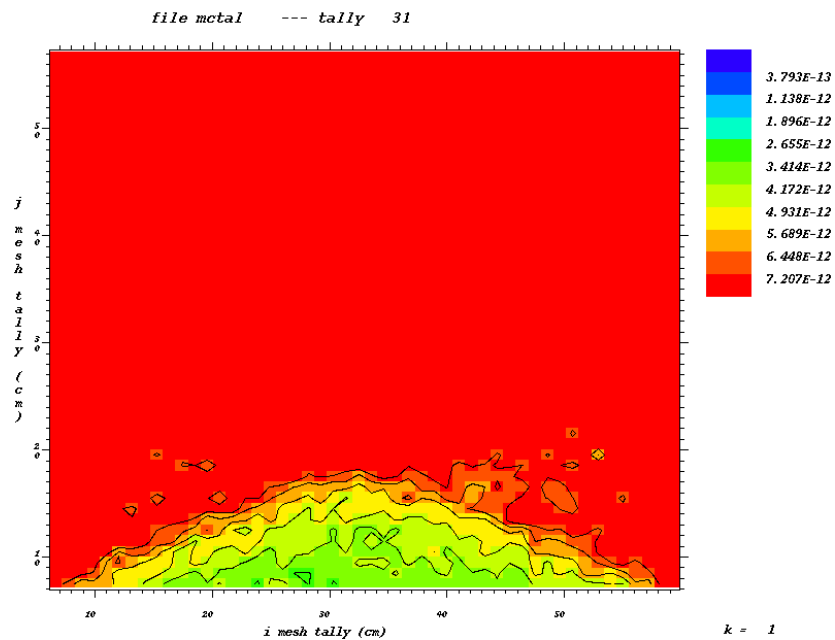


Figure III.20. Distribution of averaged absorbed dose from single source photon in Plane C. This dose distribution pattern was similar to distribution observed in Plane A and B.

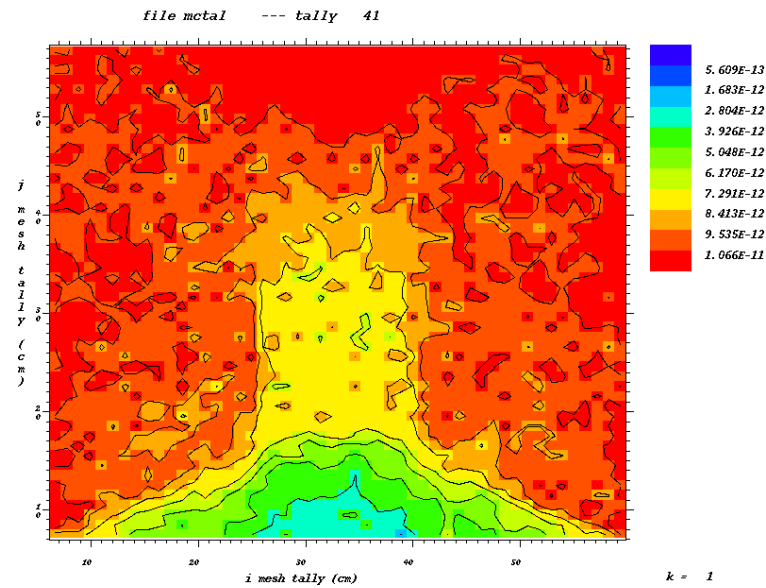


Figure III.21. Distribution of averaged absorbed dose from single source photon in Plane D. Similar to previous figures, the absorbed dose near the incubator door was lower than the dose in the back. Additionally, a clear silhouette of the culture vessel can be seen in this figure, due to the difference of absorbed dose.

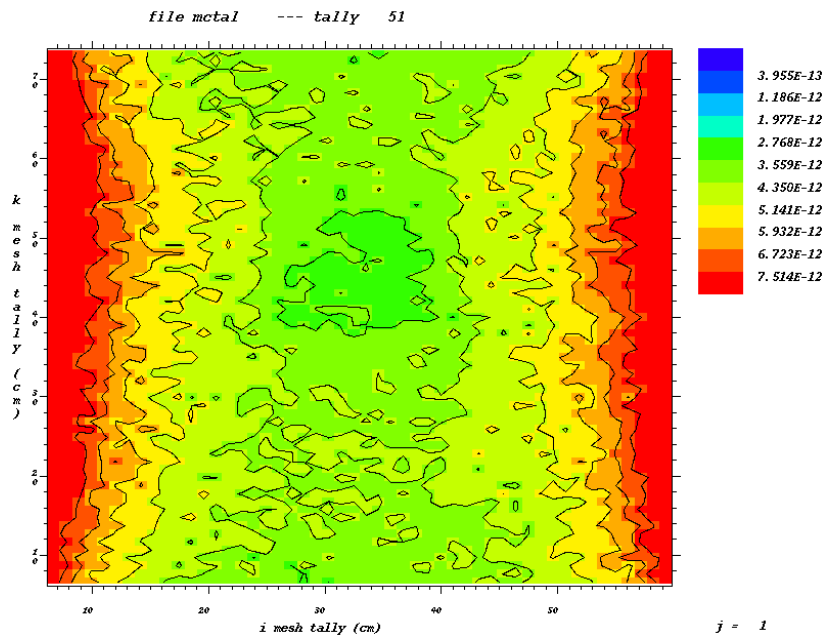


Figure III.22 Distribution of averaged absorbed dose from single source photon in Plane E. Similar to its corresponding fluence distribution, the absorbed dose was the highest at the left and right edges and was the lowest near the center.

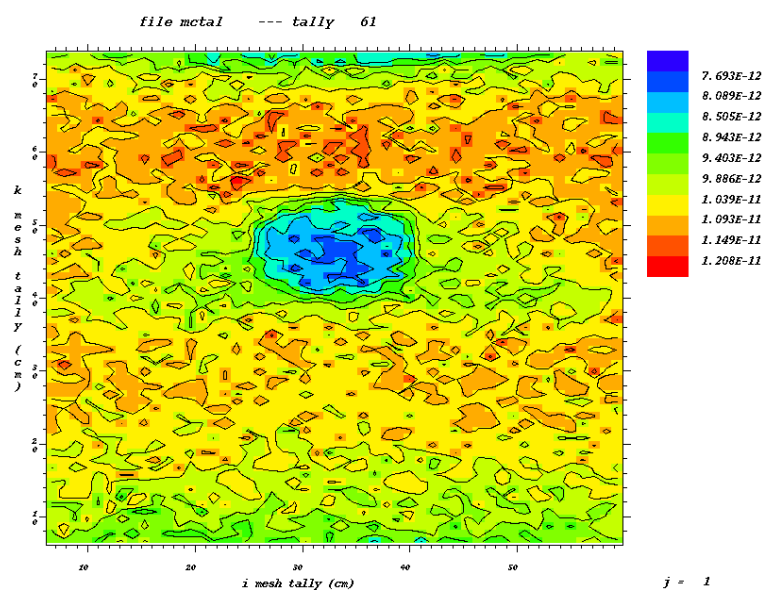


Figure III.23. Distribution of averaged absorbed dose from single source photon in Plane F. A clear silhouette of the culture vessel can be seen in this figure, due to differences in absorbed doses between the vessel and its surroundings. Magnitude wise, the absorbed dose in this figure was higher than Figure III.22 but lower than Figure III.24.

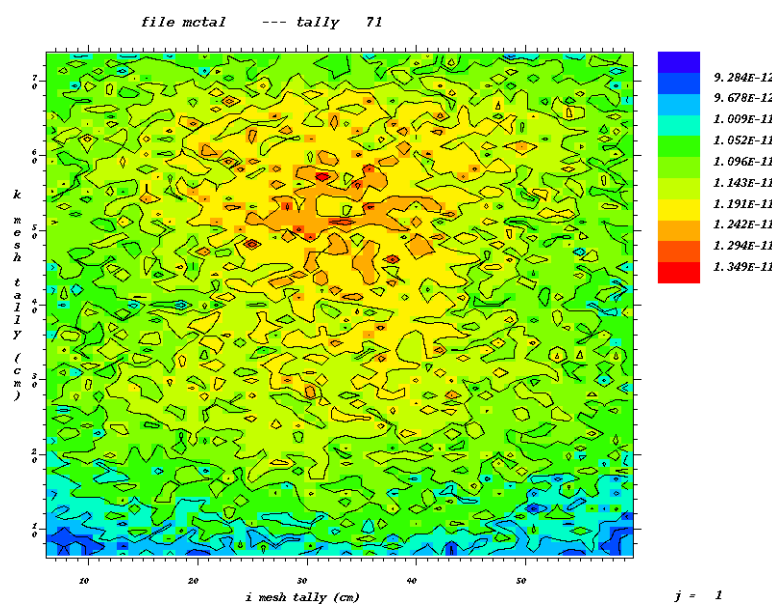


Figure III.24. Distribution of averaged absorbed dose from single source photon in Plane G. Absorbed dose was the lowest near the bottom and was highest around 50 cm height. The absorbed dose in this figure was higher than both Figure III.22 and III.23.

For the fifteen points of interest illustrated in Figure III.1, their averaged absorbed dose from a single source photon is summarized in Table III.10.

Table III.10. MCNPX simulation of averaged absorbed dose from single source photon at various locations

Point of Interest	Averaged Absorbed Dose from Single Particle (Gy)
1	2.67E-17
2	2.59E-17
3	2.21E-17
4	2.22E-17
5	2.66E-17
6	2.66E-17
7	2.43E-17
8	2.40E-17
9	2.42E-17
10	2.38E-17
11	1.96E-17
12	1.97E-17
13	2.07E-17
14	2.02E-17
15	1.95E-17

As mentioned in the previous section, the experiment used three cobalt wires with combined activity of 69 mCi (2.553E9 Bq). Because one becquerel is one disintegration per second, and each disintegration emits two photons. The absorbed dose rate of each point of interest can be obtained by multiplying its corresponding averaged single photon absorbed dose by the photon emitting rate, which is the activity in becquerel times two. The result has a unit of gray per second (Gy/s), which can be easily converted to gray per hour (Gy/h). Since each experimental measurement lasted eight hours, the total absorbed dose at each point of interest can be acquired by multiplying

dose rate (Gy/h) by the experiment duration (h). The number of photons emitted in eight hours is $1.47\text{E}+14$. The eight hours total absorbed dose at each point of interest and their respective relative error is summarized in Table III.11.

Table III.11. Comparison of MCNPX simulation and measured results of total absorbed dose in eight hours

Point of interest	MCNPX simulation result (Gy)	Relative error	Measured result (Gy)	Relative error	Ratio (Measured/simulation)
1	3.92E-03	1.23%	4.24E-03	14.92%	1.08
2	3.80E-03	0.68%	3.72E-03	19.53%	0.98
3	3.26E-03	1.17%	3.34E-03	9.50%	1.03
4	3.26E-03	1.18%	3.97E-03	9.10%	1.22
5	3.92E-03	0.73%	3.47E-03	10.94%	0.89
6	3.90E-03	0.71%	3.92E-03	16.17%	1.00
7	3.58E-03	1.06%	3.51E-03	13.94%	0.98
8	3.52E-03	0.69%	3.84E-03	8.96%	1.09
9	3.56E-03	1.47%	3.19E-03	18.09%	0.90
10	3.50E-03	0.89%	5.62E-03	34.39%	1.61
11	2.88E-03	1.32%	3.50E-03	30.11%	1.22
12	2.90E-03	1.43%	2.87E-03	12.60%	0.99
13	3.04E-03	0.62%	3.38E-03	15.22%	1.11
14	2.98E-03	0.81%	3.92E-03	22.79%	1.32
15	2.88E-03	0.58%	3.08E-03	11.84%	1.07

IV. DISCUSSION

Due to the inherent errors of performing the actual experiment, such as the uneven heating in the TLD reader and radiation from the reactor, the MCNPX simulation is considered more accurate in comparison. Based on results shown in previous sections, the data from the actual experiment agreed with the MCNPX simulation in both dose distribution pattern and magnitude.

In the MCNPX simulation, as evidenced in Figures III.18, III.19 and III.20, the absorbed dose distributions are mostly uniform for spaces away from the incubator door, which made up the majority of the incubator volume. All three figures showed the dose was lowest right behind the center line of incubator door, and gradually increased toward the back and left and right edges. Based on readings from the three figures, the dose minimum was 50% - 60% lower than the dose maximum in their respective horizontal planes. This distribution pattern can be explained by the difference in stopping power for different materials. The door and the other walls have about the same thickness, however, the door is composed only of fiberglass while the walls are composed of water and fiberglass. Because fiberglass has higher Z number than water, hence, it has higher attenuation factor. As a result, photons that are attenuated by the door which has a thicker fiberglass layer have lower energy, thus resulting in a lower interior dose behind the door. Despite this large difference in magnitude around the door area, all the horizontal figures showed that only a small percentage (around 10%) of the incubator volume was affected by the door. For space not affected by the door, dose distribution

can be considered uniform. This was evidenced in Table IV.1, dose in the rear space was only 15% higher than dose in front on average, and for individual Planes A, B and C, differences for dose at all points of interest were well below 20%.

Table IV.1. Comparison of total absorbed dose between frontal and rear TLDs for the actual experiment and simulation

	Front vs. Rear	Simulated	Actual
Plane A	3 vs. 2	14.21%	10.07%
	4 vs. 1	16.84%	6.33%
Plane B	7 vs. 6	8.21%	10.30%
	8 vs. 5	10.20%	-10.69%
Plane C	11 vs. 10	17.71%	37.72%
	12 vs. 9	18.54%	9.88%
average		14.29%	10.60%

Such dose distribution patterns were also observed in the actual experiment. Most of the frontal TLDs (# 3, 4, 7, 8, 11 and 12) recorded lower doses than the TLDs in the back (# 1, 2, 5, 6, 9 and 10). Magnitude-wise, as shown in Table IV.1, the actual experiment exhibited an even more uniform distribution pattern than the MCNP simulation. On average, dose in the rear space was only 10% higher than dose in the front, compared to the 15% in simulation.

The upper horizontal plane (Plane A), which TLD # 1, 2, 3 and 4 rest upon, was comparable to its corresponding MCNPX plane profile, where TLD # 3 (front, right) is lower than TLD # 2 (rear, right) by 10.07% versus the 14.21% in the simulation and TLD # 4 (front, left) is lower than TLD # 1 (rear, left) by 6.33% versus the 16.84% in the simulation.

The middle (Plane B) and the lower (Plane C) horizontal plane exhibit similar distribution patterns, where frontal doses are just slightly lower than the rear doses. The only exceptions were TLD # 8 (middle, right, front) being 10.69% higher than TLD # 5 (middle, right, rear).

Magnitude-wise, the dose measured in the actual experiment was very similar to the simulation value with some minor differences. Table III.11 showed the majority of experiment/simulation ratios was close to one (ranging between 0.89 to 1.32), excluding TLD#10, which had a ratio of 1.61. This inconsistency was likely due to the location of TLD#10 being closest to the nuclear reactor during the experiment, but it can also be possibly caused by a combination of several factors, namely, TLD errors and the inconsistency of incubator material distribution.

The unusually large dose reading in TLD#10, along with abnormal ratio between TLD #8 and #5, suggests the possibility of TLD errors. Subsequent post-experiment tests placed the fifteen TLDs in the same spot within the incubator for eight hours, and the result showed abnormal exposure readings for the three TLDs in question, hence confirming some degree of inconsistency amongst the TLD chips. The result of post-experiment tests can be found in Appendix B.

Another explanation for actual dose being different than the simulation is the background radiation from the reactor. As shown in previous calculations, radiations from the cobalt wires are responsible for the vast majority of radiation dose. However, background radiation was accountable for about 10% of the total dose registered in the TLD chips. Therefore, background radiation can be considered at least a minor factor

causing the discrepancy, especially for TLD#10 since it was the nearest to the nuclear reactor.

The final explanation is the inconsistency of incubator material. In MCNPX simulation, only three materials, namely, stainless steel, fiberglass and water were considered as the incubator building materials. However, in reality, there may be more types of materials that were used to construct the incubator, such as tin coating, copper wiring and/or other metallic components. These materials have the potential to influence the radiation field differently due to the difference in attenuation factors.

Despite the small discrepancies between the MCNPX simulation and the actual experiment, the majority of the points of interest shared many similarities in terms of distribution pattern and magnitude. Both the simulation and the experiment suggested the dose distribution in rear incubator volume was uniform. Due to striking resemblance between the simulation and the experiment, one can further imply that if the bacteria culture vessel was available at the time of experiment, the dose distribution within its boundary would also be uniform, as suggested in the MCNPX simulation.

V. CONCLUSION AND FUTURE WORK

V.A Conclusion

The objective of this research was to create a uniform radiation environment with a dose rate below 1 mGy/h. To accomplish this task, MCNPX simulation was first used to test the feasibility of constructing such environment with available equipment. Once the feasibility was confirmed, an actual experiment was carried out by carefully following the simulation. To ensure the experiment consistency, fifteen TLD chips were used to monitor the radiation field for a duration of thirty days. The actual dose distribution pattern was observed to be similar to its simulation counterpart, where the dose rate near the incubator door was lower than the dose rate near the rear. A uniform radiation field was achieved in the rear space of the incubator, which accounted for the majority of the incubator volume. Furthermore, the actual dose rate had a range from 0.298 to 0.696 mGy/h, hence meeting the initial design criteria.

V.B Future Work

Several improvements can be made to enhance the accuracy of future experiments. First is TLD selection. As TLD chip detection efficiency depends on its material makeup, TLDs from different manufacturer will have some difference in material composition, hence they may produce inconsistencies in dose readings. Even for TLDs from the same manufacturer, there are still significant variations, known as "batch variations". Therefore, mix matching of TLDs from different manufacturer is not

recommended. If financially possible, one can irradiate a large number of TLDs and select those with the same response to overcome the inherent variations.

The second recommendation concerns experiment site selection; an ideal site for this experiment is a location with very low background radiation. Places near the nuclear reactor or radioactive materials are not recommended.

The third recommendation is to spread the source more evenly around the incubator. Within financial constraints, one can use more cobalt wires with less activity to create a more uniform radiation field. For example, using six wires each with half the activity would result a more homogeneous radiation field than the setup used in this research. If the experiment site allows liquid to be as used radiation source, one can use the MIT approach mentioned in the introduction section by mixing radioactive material into liquid and inject the newly created liquid source into the incubator water jacket to produce an even more uniform radiation field.

The ultimate purpose of this research is to examine the feasibility of constructing a low-dose irradiation facility to simulate the exposure rates that exist in space. Cosmic rays consist of protons, alpha particles, beta particles, gamma rays and heavier ions. Hence, using a gamma source is only the first step to simulate a realistic space environment on Earth. For particles that have short range, such alpha and heavy ions, the source may be positioned inside the incubator near the bacterial vessel (target). For particles that have a longer range, the sources may be positioned outside of the incubator.

REFERENCES

Attix FH. Introduction to radiological physics and radiation dosimetry. New York: John Wiley and Sons; 2004.

Beckurts KH, Wirtz K. Neutron physics. New York: Springer-Verlag; 1964.

Berger T., Hajek M. TL-efficiency—Overview and experimental results over the years, *Radiation Measurements*, 43:146-156; 2008.

Cucinotta F. Space radiation organ dose for astronauts on past and future missions. Available at http://ntrs.nasa.gov/archive/nasa/casi.ntrs.nasa.gov/20070010704_2007005310.pdf. Accessed 5 December 2010.

Guan F. Design and simulation of a passive-scattering nozzle in proton beam radiotherapy. M.S. thesis, Texas A&M University, College Station; 2009.

Howell RW, Goddu M and Rao DV, Design and performance characteristics of an experimental cesium-137 irradiator to simulate internal radionuclide dose rate patterns, *Journal of Nuclear Medicine*, 38: 727-730; 1997.

International Commission on Radiation Units and Measurements (ICRU). Radiation Quantities and Units, ICRU Report 47. Bethesda, MD: Int. Comm. Radiat. Units and Measurement; 1992.

International Commission on Radiological Protection (ICRP). A Framework for Assessing the Impact of Ionising Radiation on Non-human Species, ICRP Publication 91.; 2003.

Ishida Y, Takabatake T, Kakinuma S, Doi K, Yamauchi K, Kaminishi M, Kito S, Ohta Y, Amasaki Y, Moritake H, Kokubo T, Nishimura M, Nishikawa T, Hino O, Shimada Y. Genomic and gene expression signatures of radiation in medulloblastomas after low-dose irradiation in Ptch1 heterozygous mice. *Carcinogenesis* 31:1694-1701.; 2010.

Mayo RM. Introduction to nuclear concepts for engineers. La Grange Park, IL: American Nuclear Society; 1998.

Mihok S. Chronic exposure to gamma radiation of wild populations of meadow voles. *Journal of Environmental Radioactivity*, 75: 233-266; 2004.

Mishev AL, Mavrodiev SC and Stamenov JN. In Martsch IN eds. *Frontiers in cosmic rays research*, New York: Nova Science Publishers, 35-83; 2004.

Mitchel R EJ, Burchart P and Wyatt H. A lower dose threshold for the in vivo protective adaptive response to radiation. Tumorigenesis in chronically exposed normal and Trp53 heterozygous C57BL/6 mice, Radiation Research Society; 170:765-75;2008.

Oldenberg, O., Rasmussen, NC. Modern physics for engineers. New York: McGraw-Hill, Inc; 1996.

Olipitz W, Hembrador S, Davidson M, Yanch JC, Engelward BP. Development and characterization of a novel variable low dose-rate irradiator for in vivo mouse studies. Health Physics Society, 2010.

Rice AJ. Mathematical statistics and data analysis, 2nd ed. Belmont, CA, Duxbury Press; 1995.

Shin SC, Lee KM, Kang YM, Kim K, Kim CS, Yang KH, Jin YW, Kim CS, Kim HS. Alteration of cytokine profiles in mice exposed to chronic low-dose ionizing radiation. Biochemical and Biophysical Research Communications, 2010.

Simpson JA, Elemental and isotopic composition of the galactic cosmic rays, Nucl. and Particle Sci., 33:323-382; 1983.

Thermo Scientific Forma Series II Water Jacketed CO₂ Incubator, Thermo Scientific. Available at: <http://www.thermoscientific.com/wps/portal/ts/products/detail?productId=11962287>. Accessed 11 February 2011.

Tsoufanidis N., Measurement and detection of radiation, 2nd ed. Washington, DC: Taylor & Francis; 1995.

Turner JE. Atoms, radiation and radiation protection, 2nd ed. New York: Wiley & Sons; 1995.

Wakeford R, Tawn EJ, The meaning of low dose and low dose-rate. Journal of Radiological Protection, 30: 1-3; 2010.

APPENDIX A

MCNPX Input Used to Generate the Geometry and to Calculate Fluence and Dose

```

c      Created on: Thursday, Sep 09, 2010 at 11:00am
1      0      1  $outer space
2      2      -2.5 -2  $door
3      2      -2.5 -3  $top
4      2      -2.5 -4 5  $fiber glass
5      1      -1 -5 6  $water
6      3      -7.92 -6 7  $steel inner
7      4      -.001225 -7 #9 #10  $incubator space
8      4      -.001225 -1 #2 #3 #4 #5 #6 #7 #9 #10  $roomair
9      3      -3.96 -8  $steel rack
10     1      -1 -9  $culture vessel

1      so 500
c      door
2      rpp 0 66 0 6.75 0 80.3
c      top
3      rpp 0 66 0 63.5 80.3 100.3
c      fiber glass outer
4      rpp 0 66 6.75 63.5 0 80.3
c      fiber glass inner& water outer
5      rpp 2.3 63.7 6.75 61.2 2.3 77.7
c      water inner
6      rpp 5.95 60.05 6.75 57.55 5.95 74.05
c      steel inner
7      rpp 6.15 59.85 6.95 57.35 6.15 73.85
c      steel rack
8      rpp 6.16 59.84 6.96 57.34 39.9 40.1
c      culture vessel
9      rcc 33 18.15 47.1 0 28 0 7

mode p
c h2o
m1     1000.      2  $MAT1
      8000.      1
c SiO2 2.5 g/cm3
m2     14000.    1  $MAT2
      8000.      2
c stainless steel 304 7.92g/cm3
m3     24000.    -0.19 $MAT3
      25055.    -0.02 26000.      -0.695 28000.
-0.095
c      air (US S. Atm at sea level)      ,d=-.001225      ,HC&P 14-19
m4     7000.      -0.7556360
      8000.      -0.2314750 18000.      -0.0128890
imp:p  0      1 8r      $ 1, 10
sdef pos d1 erg d3 axs 0 0 1 rad d4 ext d5 wgt 1

```

```

c the activity of 1 m co 60wire is 8.51e8 Bq = 3.06e12/h,
c there are 3 wires, total activity is 2.553e9 Bq = 9.191e12/h
c irradiating 8 hrs, the # of decays of Co60 is 7.353e13
c 2 photons(1.173 and 1.332 MeV) are emmitted in each decay
c the total # of photons is 1.471e14 in 8 hrs
sil L 33 131.5 50 -53.6 -18.5 50 119.6 -18.5 50 $1m*3
spl 1 1 1
si3 L 1.173 1.332
sp3 1 1
si4 0 0.025
sp4 -21 1
si5 -50 50
sp5 -21 0
c tally card
c top plane
f15:p 6.35 57.15 73.65 0
f25:p 59.65 57.15 73.65 0
f35:p 59.65 7.15 73.65 0
f45:p 6.35 7.15 73.65 0
c middle plane
f55:p 6.35 57.15 40.3 0
f65:p 59.65 57.15 40.3 0
f75:p 59.65 7.15 40.3 0
f85:p 6.35 7.15 40.3 0
c bottom plane
f95:p 6.35 57.15 6.35 0
f105:p 59.65 57.15 6.35 0
f115:p 59.65 7.15 6.35 0
f125:p 6.35 7.15 6.35 0
c in the cylinder
f135:p 33 35.15 47.1 0
f145:p 33 32.15 47.1 0
f155:p 33 29.15 47.1 0
c f4:p 10 $ cell flux
c f6:p 10 $ absorbed dose
c ICRP74-p159 table A.1 fluence to air-kerma conversion coefficients
c photon energy (MeV) Ka/phi (pGy cm2)log-log
de0 0.01 0.015 0.02 0.03 0.04 0.05 0.06 0.08
    0.1 0.15 0.2 0.3 0.4 0.5 0.6 0.8
    1.0 1.5 2.0 3.0 4.0 5.0 6.0 8.0
    10.0
df0 7.43 3.12 1.68 0.721 0.429 0.323 0.289 0.307
    0.371 0.599 0.856 1.38 1.89 2.38 2.84 3.69
    4.47 6.14 7.55 9.96 12.1 14.1 16.1 20.1
    24.0
c mesh tally, flux in unit volume of material,
c and dose with conversion fun. ICRP-21 1971
c 6.15 59.85 6.95 57.35 6.15 73.85
tmesh
  rmesh11:p flux dose
  cora11 6.15 49i 59.85
  corb11 6.95 49i 57.35
  corc11 73.35 73.85
  rmesh21:p flux dose

```

```
cora21 6.15 49i 59.85
corb21 6.95 49i 57.35
corc21 40.0 40.5
rmesh31:p flux dose
cora31 6.15 49i 59.85
corb31 6.95 49i 57.35
corc31 6.0 6.5
rmesh41:p flux dose
cora41 6.15 49i 59.85
corb41 6.95 49i 57.35
corc41 46.8 47.3
rmesh51:p flux dose
cora51 6.15 49i 59.85
corb51 6.95 7.95
corc51 6.15 66i 73.85
rmesh61:p flux dose
cora61 6.15 49i 59.85
corb61 31.65 32.65
corc61 6.15 66i 73.85
rmesh71:p flux dose
cora71 6.15 49i 59.85
corb71 56.35 57.35
corc71 6.15 66i 73.85
endmd
c running parameters
nps 1e8
print
prdmp 2j 1
```

APPENDIX B

Results of post-experiment tests

TLD Number	Exposure (nC)	Dose (R)
1	34.756	0.452
2	31.786	0.381
3	24.778	0.248
4	30.910	0.309
5	35.296	0.424
6	30.636	0.337
7	30.760	0.492
8	26.665	0.453
9	31.482	0.378
10	31.264	0.531
11	48.704	0.536
12	28.191	0.366
13	36.526	0.475
14	31.184	0.468
15	30.715	0.369

APPENDIX C

Calculation for Activity Per Cobalt Wire Used by MCNP

$$V = \pi * r^2 * h = \pi * 0.25mm^2 * 1000mm = 785mm^3 = 0.785cm^3$$

$$m = \rho * V = 8.9 \frac{g}{cm^3} * 0.785cm^3 = 6.987g$$

$$N = \frac{m}{M} * Na = \frac{6.987g}{60 \frac{g}{mol}} * 6.02 * 10^{23} mol = 7 * 10^{22}$$

$$\lambda = \frac{\ln(2)}{T_{1/2}} = \frac{\ln(2)}{4.62 * 10^4 h} = 1.5 * 10^{-5} h^{-1}$$

$$A_{max} = \lambda * N = 1.5 * 10^{-5} h^{-1} * 7 * 10^{22} = 1.05 * 10^{18} h^{-1} = 2.92 * 10^{14} Bq$$

Purity level is determined to be 0.00029% using methods described in Section II.D.

$$A = A_{max} * 0.00029\% = 2.92 * 10^{14} Bq * 0.00029\% = 8.51 * 10^8 Bq = 23mCi$$

APPENDIX D

Records of Cobalt Wire Neutron Activation Provided by Nuclear Science Center

Nuclear Science Center

Texas Engineering Experiment Station
Texas A&M University System
College Station, Texas 77843-3575

NSC Form 514

07/16/09

Approved *[Signature]*

Experimenter	<i>L. Vasudevan</i>	RFS Number	<i>10-0053</i>
License	<i>R-83</i>	Company	<i>NUSC</i>
Irradiation Location	<i>A4</i>	Purchase Order Number	<i>---</i>
Irradiation Date	<i>2/25/10</i>	Irradiation Device	<i>2T # 3</i>
Date/Time Completed	<i>25 Feb 2010 / 0726</i>	Irradiation Time	<i>12+42 (12.703 hr)</i>
Total Units Irradiated	<i>1 wire</i>	Total Actual Irradiation	<i>9.0 hr</i>
Sample Prepared By	<i>[Signature]</i>	CM Number	<i>10-0006</i>
Instructions for Release	<i>Decay for at least 4 days.</i>		

Unit Number	<i>1 (1 wire spooled around in aluminum cylinder in a tall can)</i>						
Material	<i>Co-60 wire</i>						
Unit Mass	<i>1.6596g</i>						
Isotopes	<i>Co-60</i>						
Activity per Unit @ EOI	<i>25.009 mCi</i>						
Activity per Unit @ EOD	<i>25 mCi</i>						
Total Activity @ EOD	<i>25 mCi</i>						

HP Approval	<i>Latha Vasudevan</i>	SRO Approval	<i>[Signature]</i>
-------------	------------------------	--------------	--------------------

Date	Time In	Time Out	Core Position	Hours Irradiated	Correction Factor	Effective Hours	Total Effective Hours	Total Remaining Hours
<i>2/25/10</i>	<i>0725</i>	<i>1625</i>	<i>A4</i>	<i>9.0</i>	<i>1.0</i>	<i>9.0</i>	<i>9.0</i>	<i>-</i>
<i>3/31/10</i>	<i>0755</i>		<i>A4</i>		<i>1.0</i>			

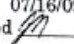
Comments	<i>Experiment will measure activity levels after decay time. Relocated into hotcell 3/31/10 [Signature]</i>
----------	---

Nuclear Science Center

Texas Engineering Experiment Station
Texas A&M University System
College Station, Texas 77843-3575


NSC Form 514

07/16/09

Approved 

Experimenter	L. Vasudevan	RFS Number	10-025
License	R-83	Company	NUEN
Irradiation Location	A-4	Purchase Order Number	N/A
Irradiation Date	12 FEB 10	Irradiation Device	Long Tube # 15
Date/Time Completed	12 Feb 10 1626	Irradiation Time	Up to 12.749 hrs
Total Units Irradiated		Total Actual Irradiation	9.33 Hrs
Sample Prepared By	A. Tijerina	CM Number	10-0006
Instructions for Release	Decay at least 4 days. Do not remove from Long Tube. 4% RSD present.		

Unit Number	1						
Material	Wire Co-60	1 m wire spool in Al cylinder in tall can.					
Unit Mass	1.5628g						
Isotopes	Co-60						
Activity per Unit @ EOI	10 mCi						
Activity per Unit @ EOD	10 mCi						
Total Activity @ EOD	10 mCi	Estimated activity. Due to self shielding effects.					

HP Approval	Latha Vasudevan	SRO Approval	
-------------	-----------------	--------------	---

Date	Time In	Time Out	Core Position	Hours Irradiated	Correction Factor	Effective Hours	Total Effective Hours	Total Remaining Hours
12 Feb 2010	0704	1626	A4	9.33	1.0	9.33	9.33	—

Comments	Release to experimenter for measuring Rad. levels when levels allow Contact Desk rate 2 R/h. @ 1 m. 28 mR/h Measurement indicate activity levels close to 20-25 mCi 2/18/10
----------	---

Nuclear Science Center

Texas Engineering Experiment Station
Texas A&M University System
College Station, Texas 77843-3575

NSC Form 514

07/16/09

Approved *[Signature]*

		RFS Number	10-084
Experimenter	L. Vasudevan	Company	NVEN
License	R-83	Purchase Order Number	—
Irradiation Location	A-4	Irradiation Device	LT # 3
Irradiation Date	31 Mar 2010	Irradiation Time	9.0 hours 12:43 hours AT
Date/Time Completed	31 Mar 2010 / 1653	Total Actual Irradiation	9.0 hr
Total Units Irradiated	4 Wires	CM Number	cm #10-0006
Sample Prepared By	A. Tijerina	RFS Prepared By	A. Tijerina
Instructions for Release Decay for at least 4 days			

Unit Number	1-4 (Co Wire spooled around an Aluminum Cylinder in a tall can x4)						
Material	Cobalt Wire						
Unit Mass	± 1.7g						
Isotopes	Co-60						
Activity per Unit @ EOI	25.009 mCi						
Activity per Unit @ EOD	25 mCi						
Total Activity @ EOD	100	125 mCi					

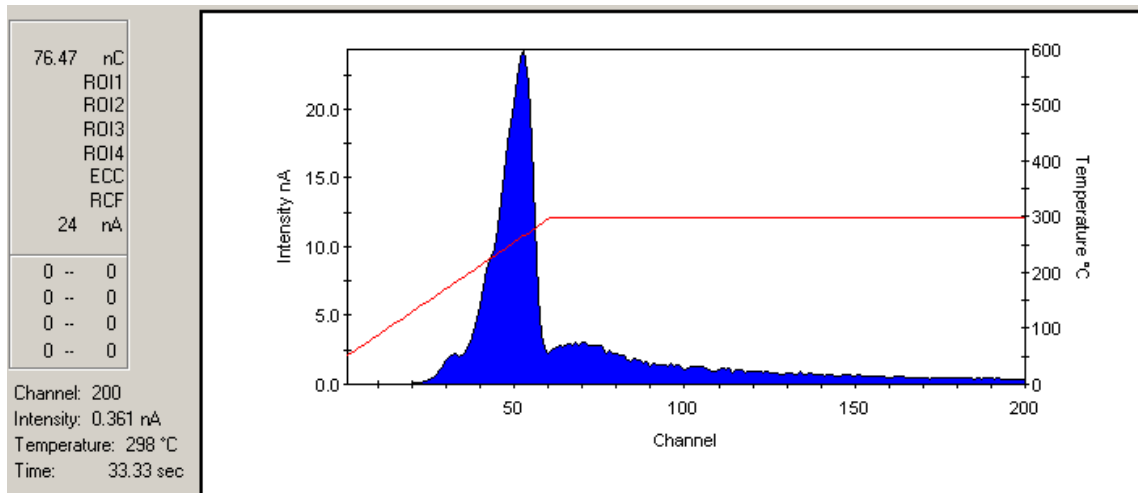
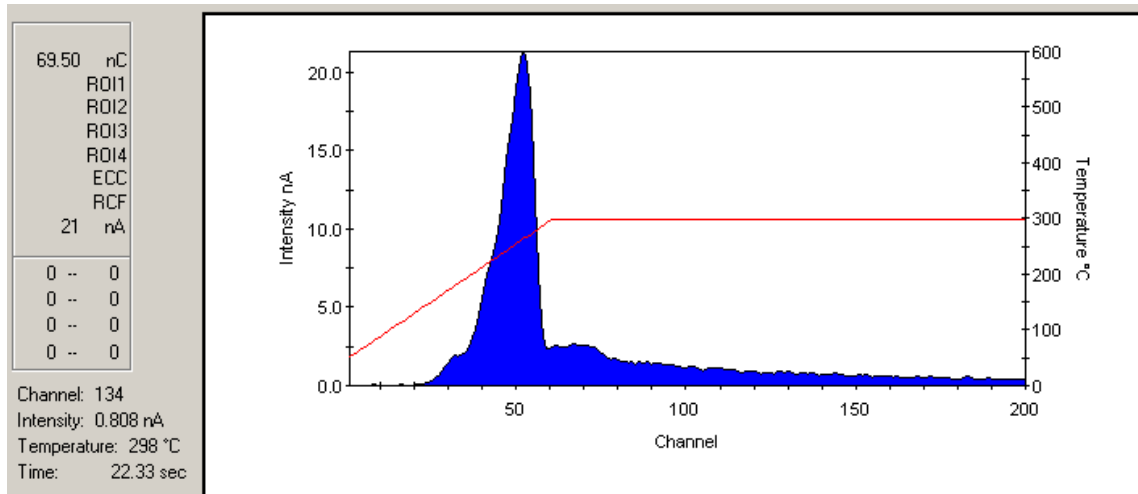
HP Approval	<i>[Signature]</i>	SRO Approval	<i>[Signature]</i>
-------------	--------------------	--------------	--------------------

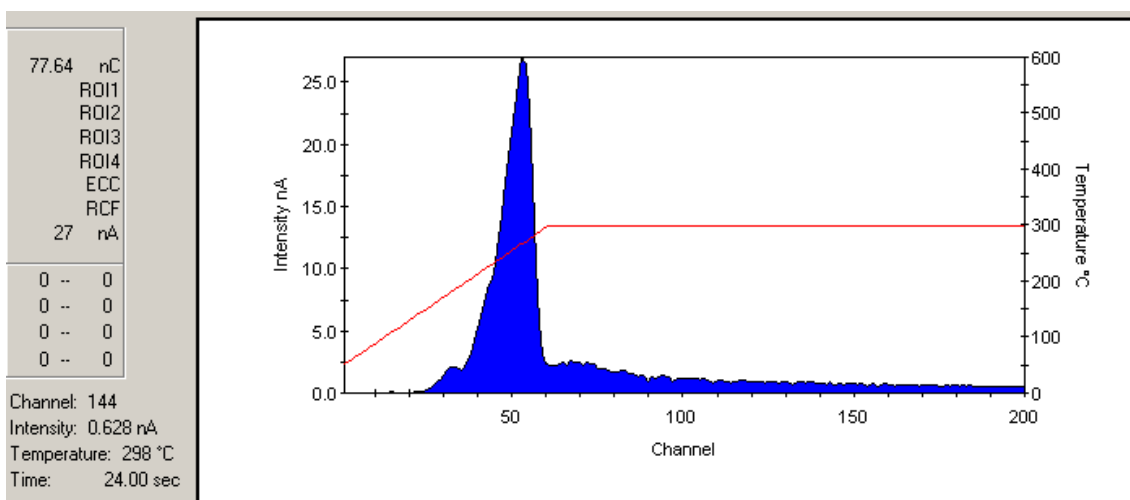
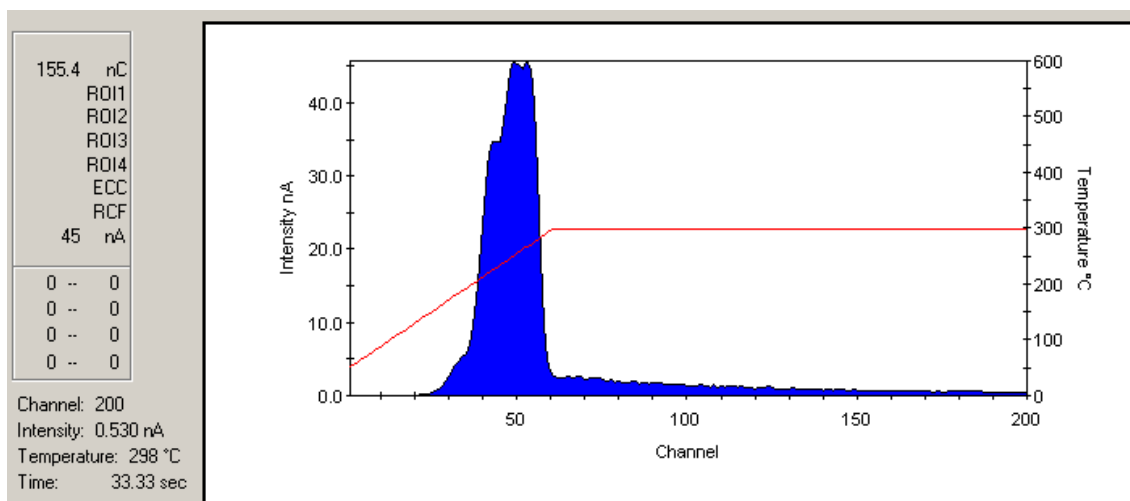
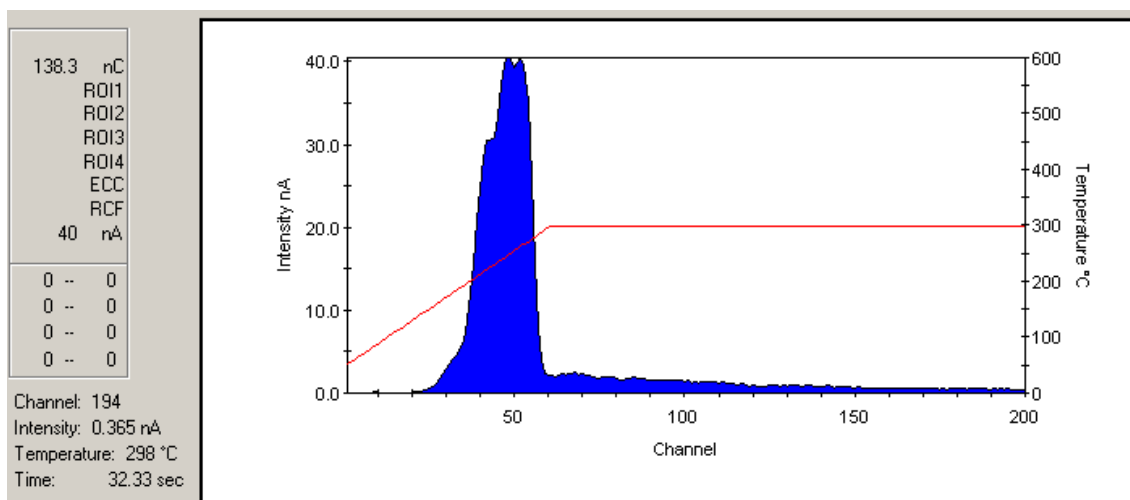
Date	Time In	Time Out	Core Position	Hours Irradiated	Correction Factor	Effective Hours	Total Effective Hours	Total Remaining Hours
31 Mar 2010	0753	1653	A4	9.0	1.0	9.0	9.0	—

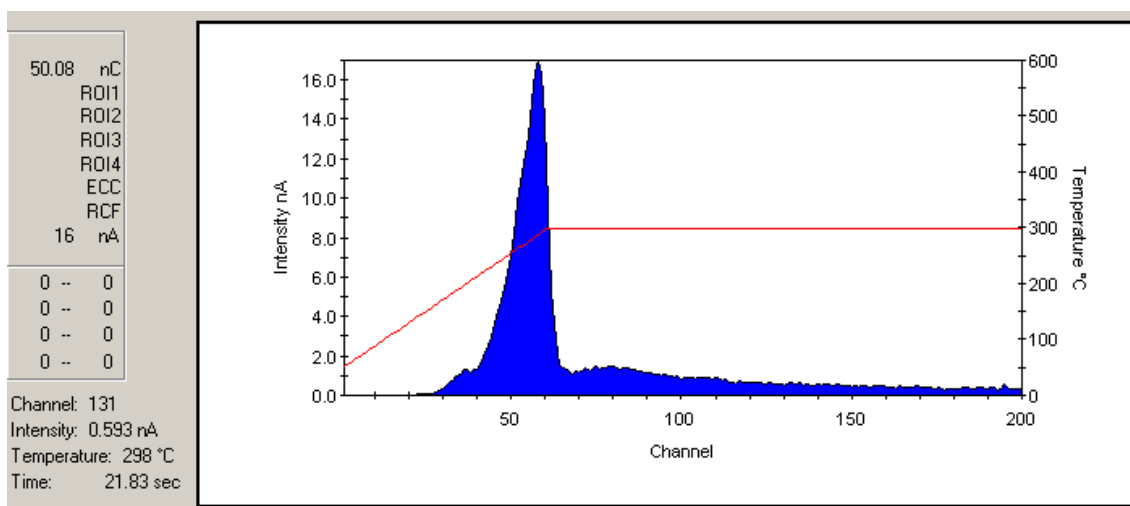
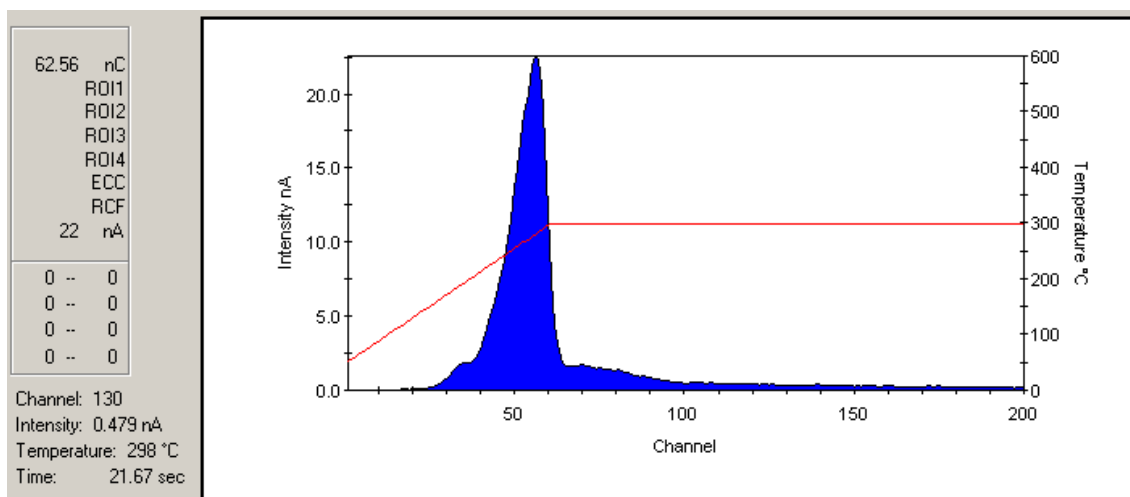
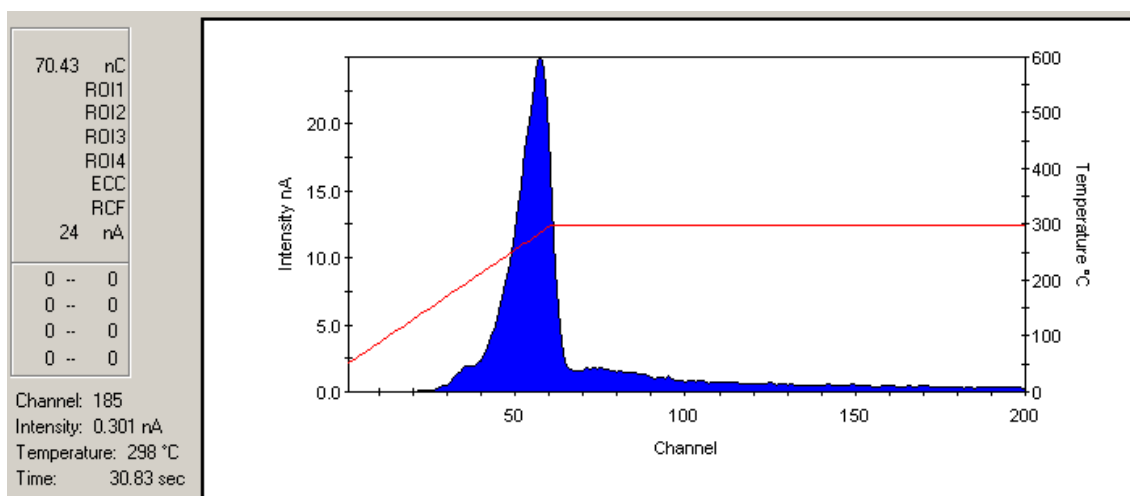
Comments	Experimenter will measure radiation levels after decay time.
----------	--

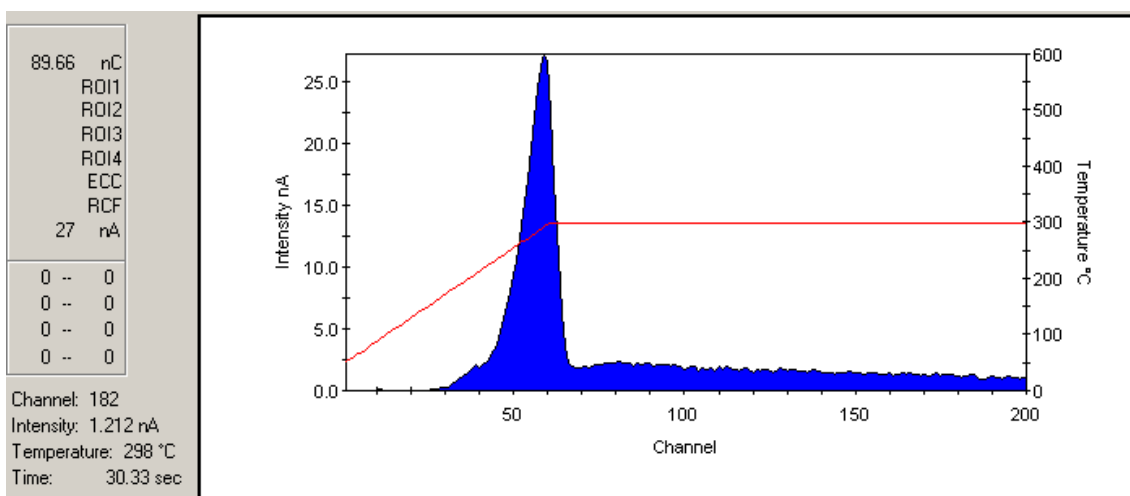
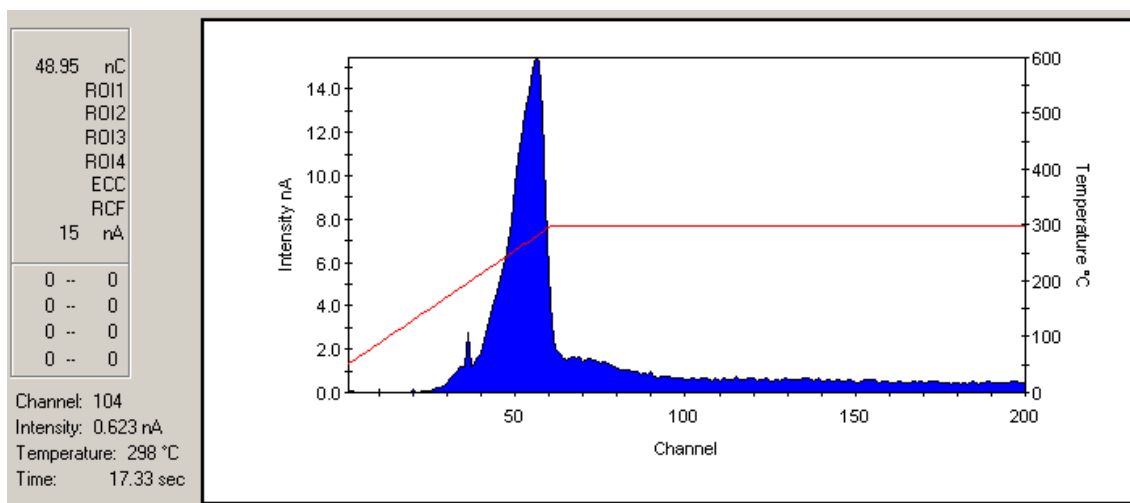
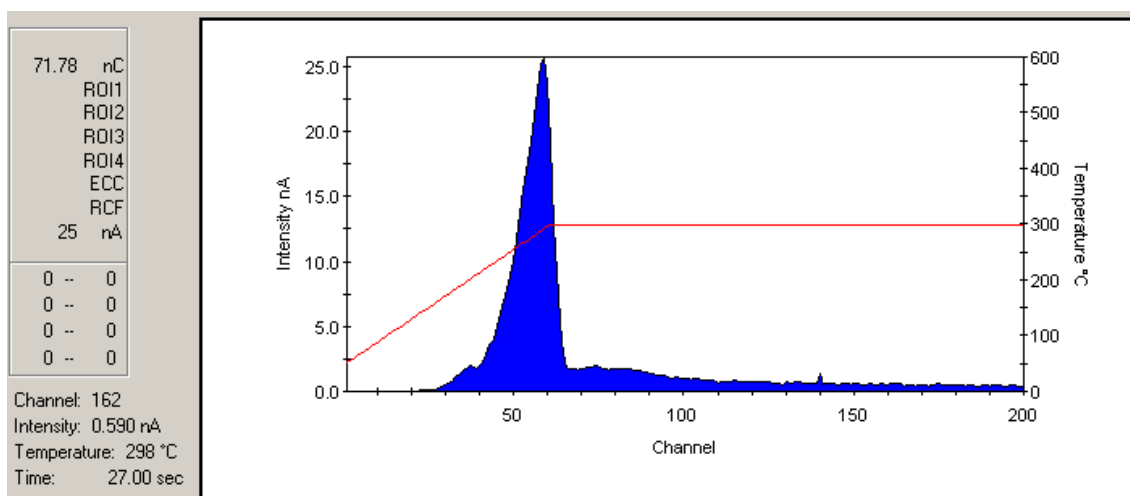
APPENDIX E

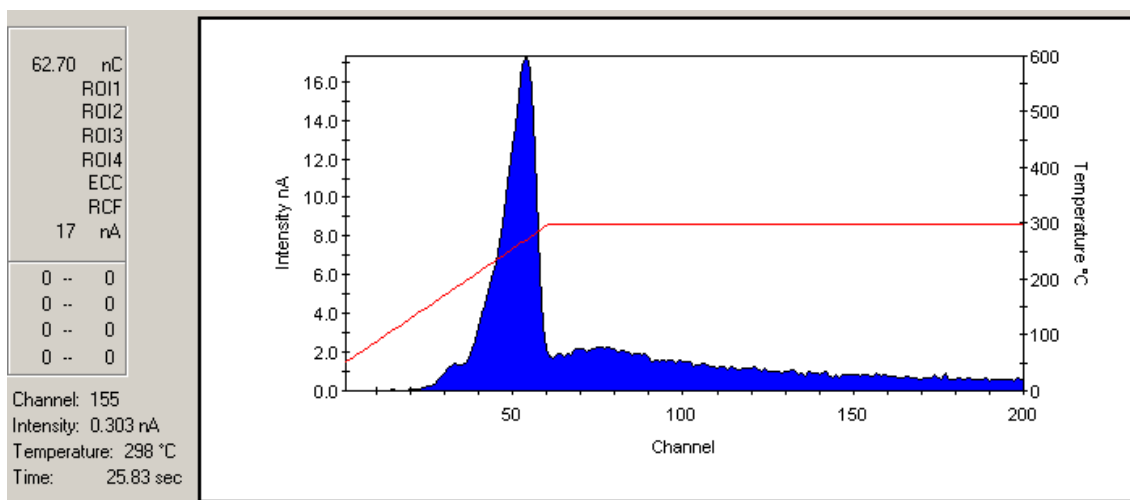
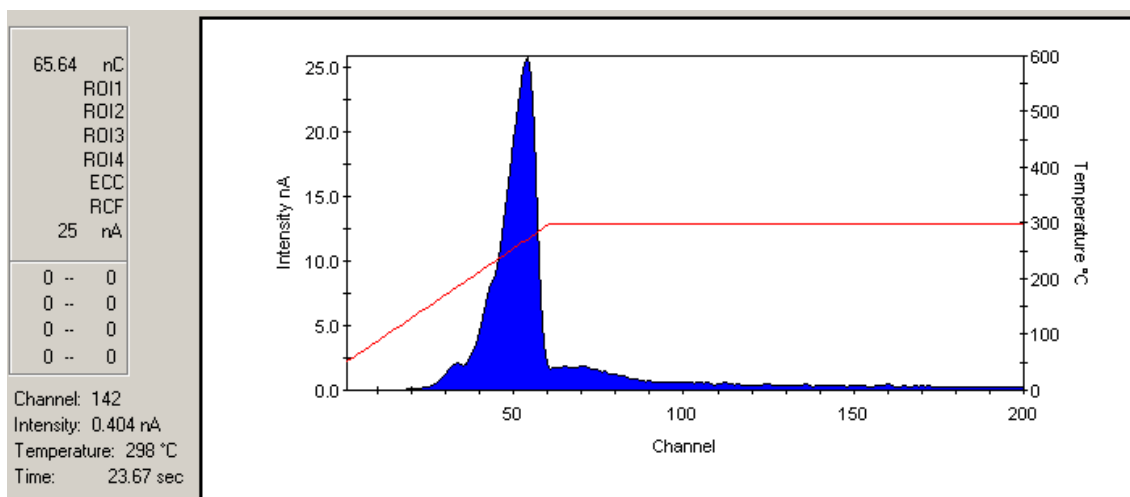
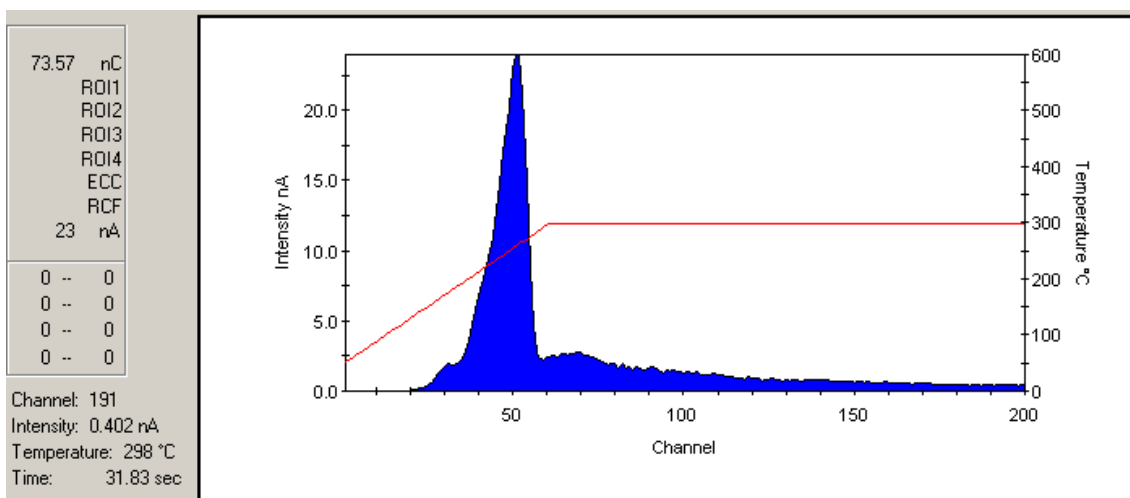
Calibration Glow Curves Generated by Exposing to 0.786 R X-Ray. Figures are Displayed in Order of TLD Number from 1 to 15.

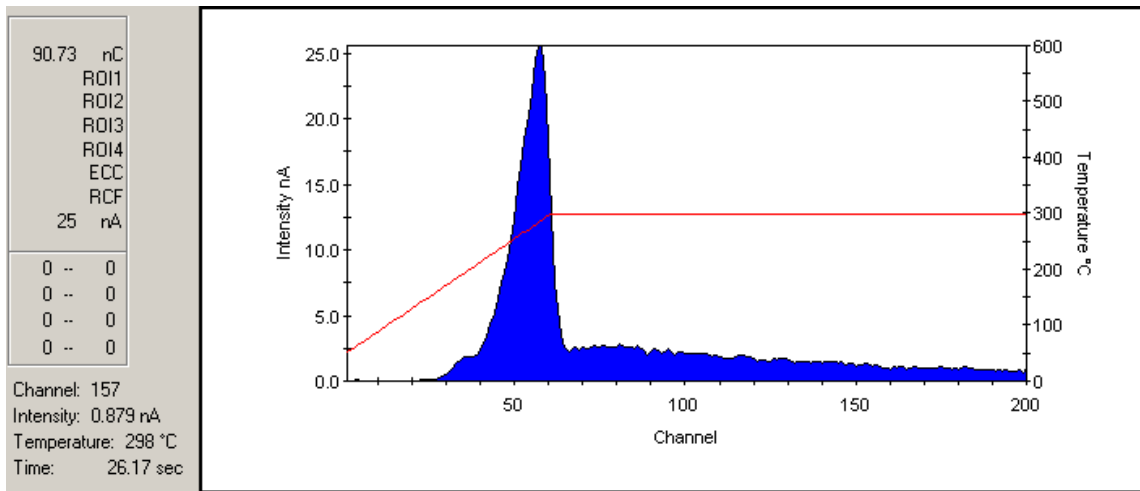






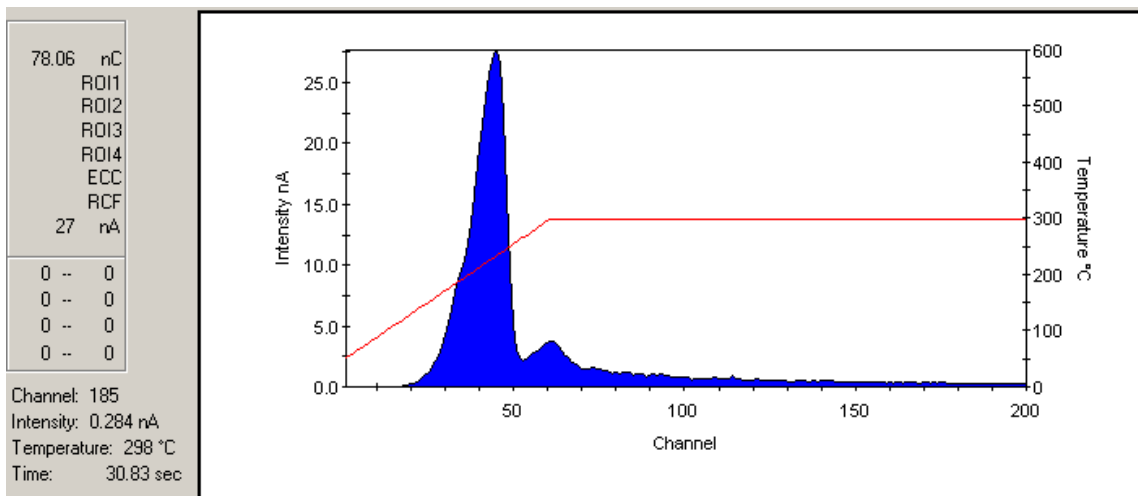
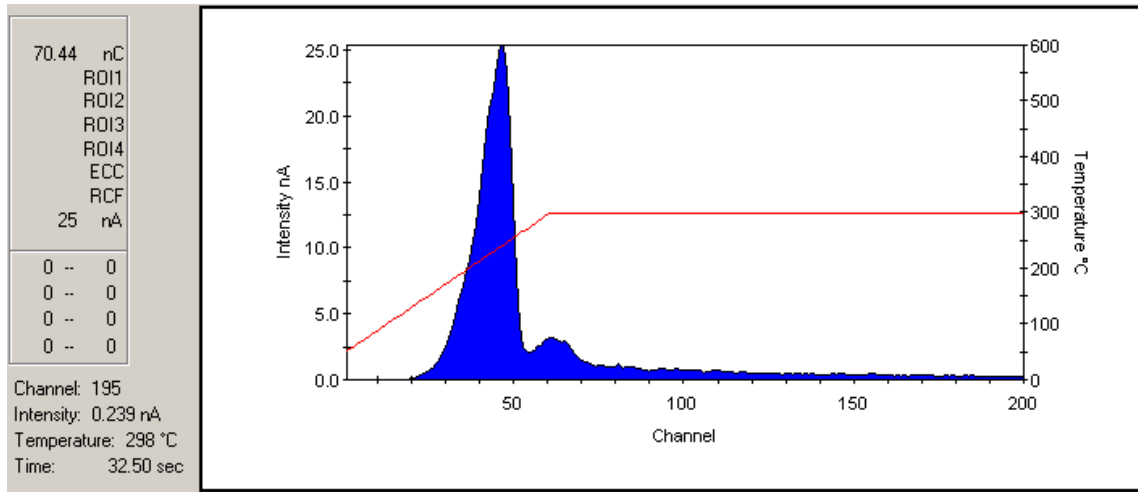


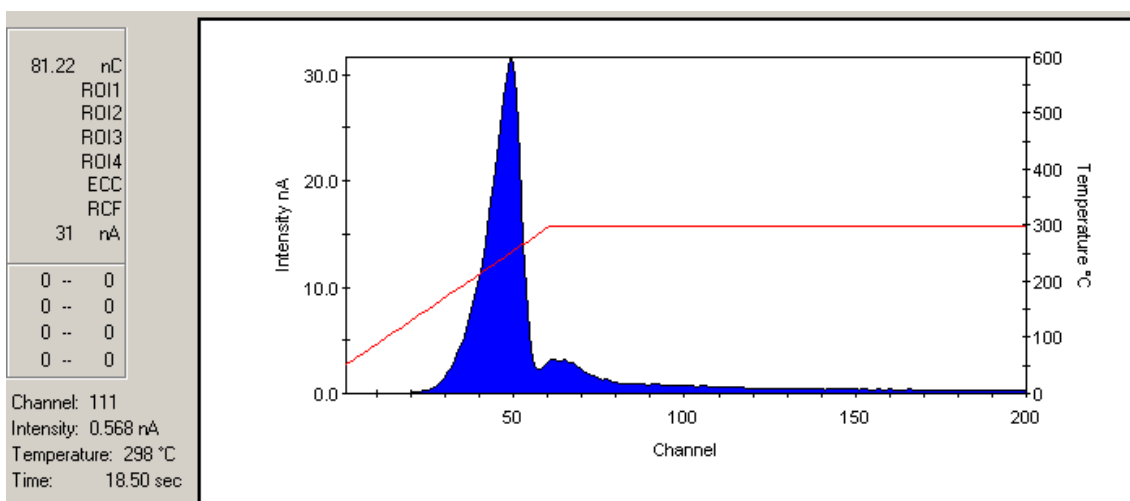
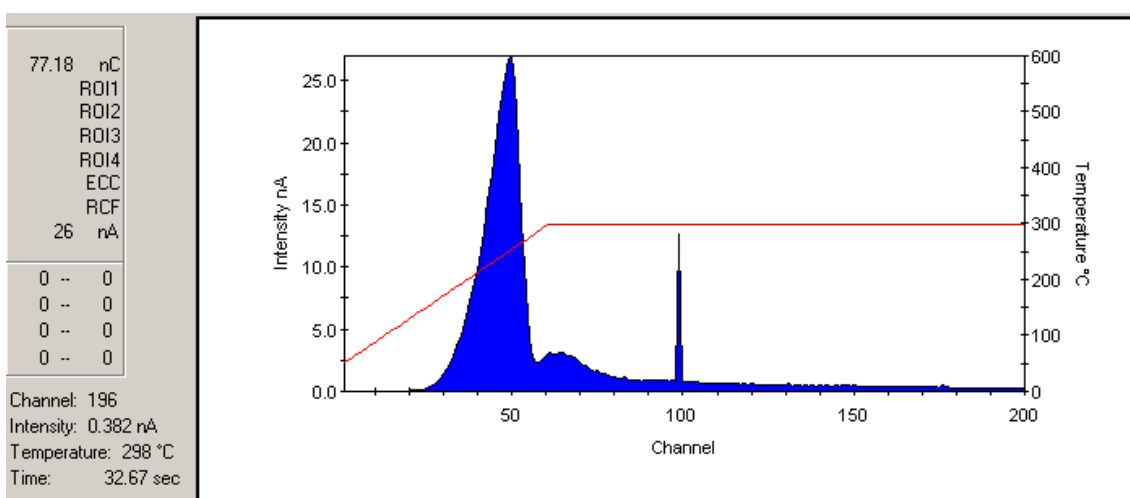
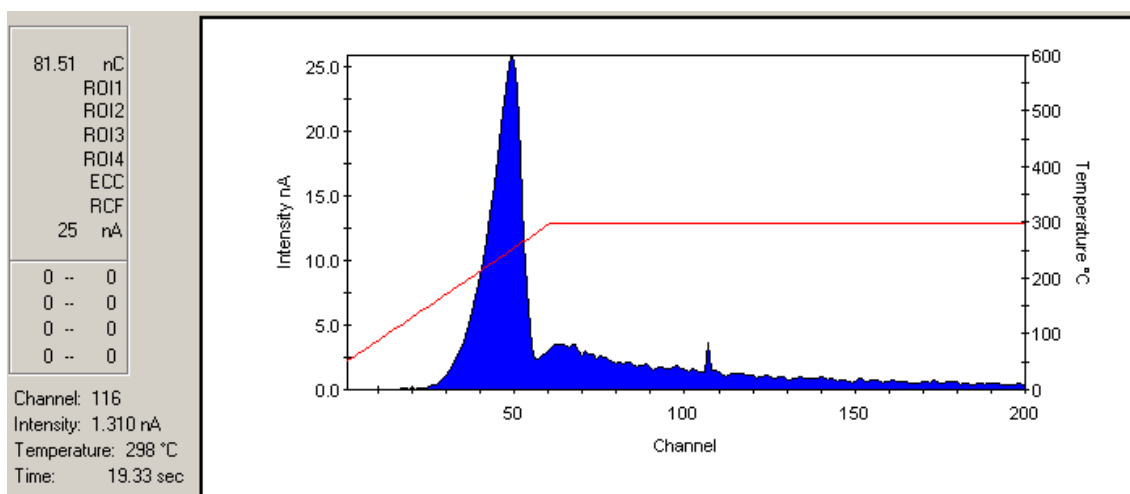


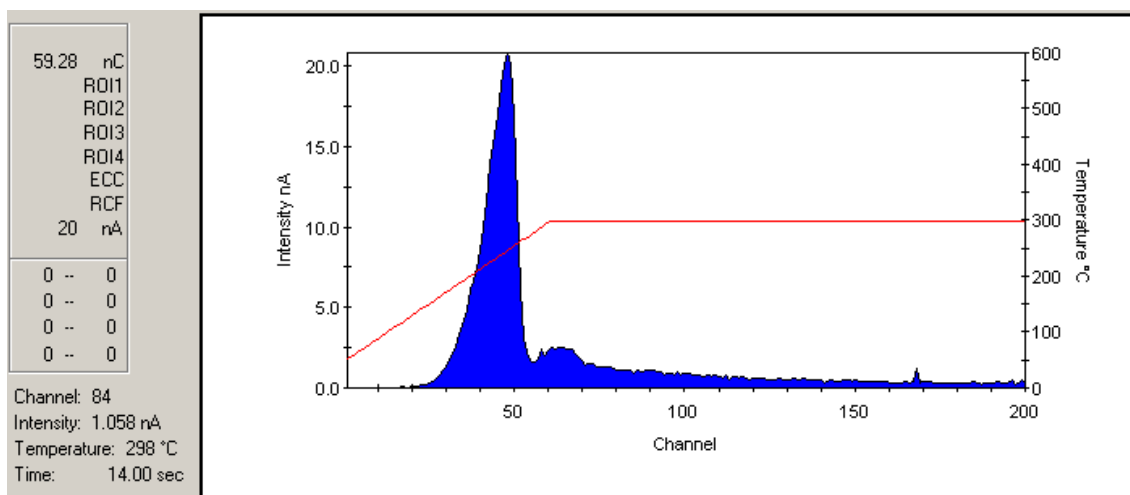
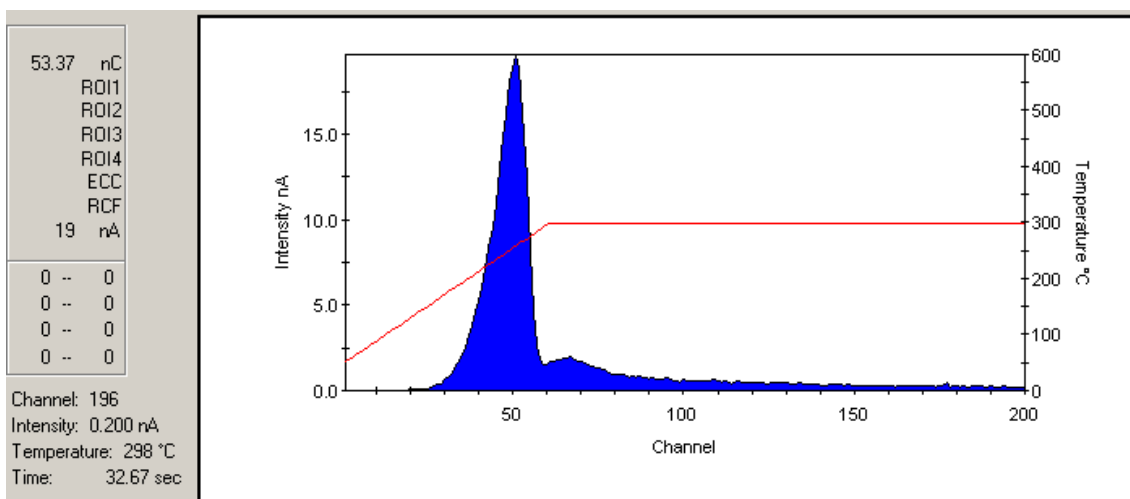
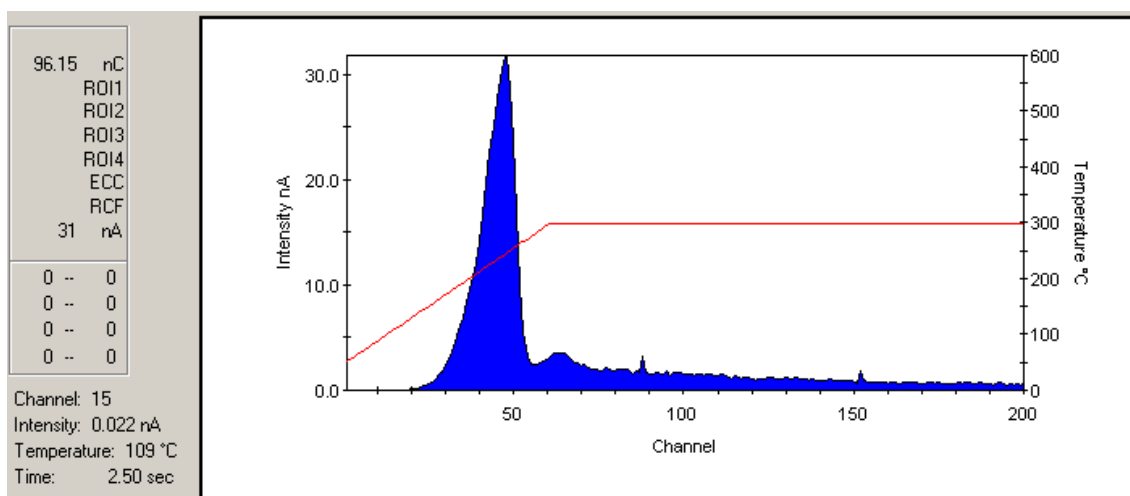


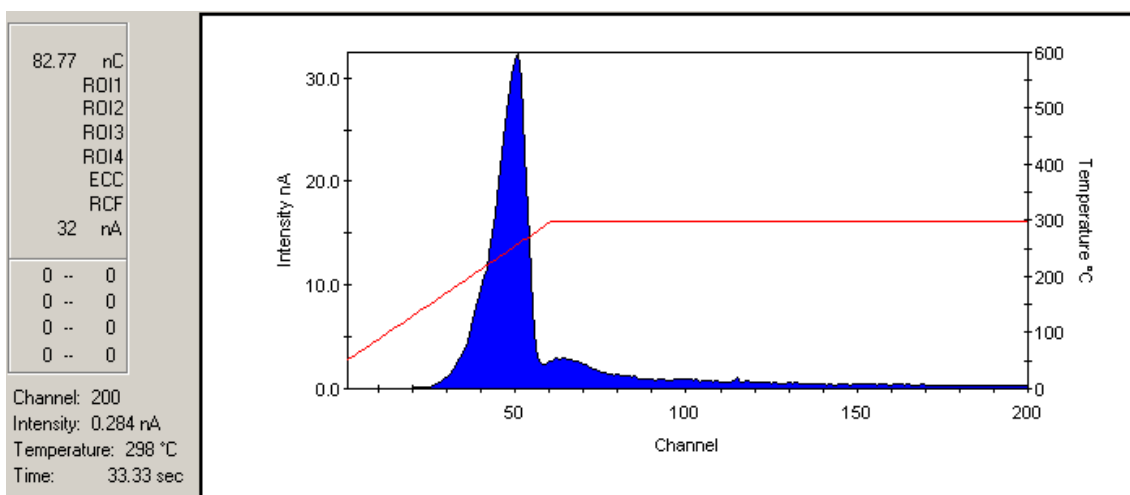
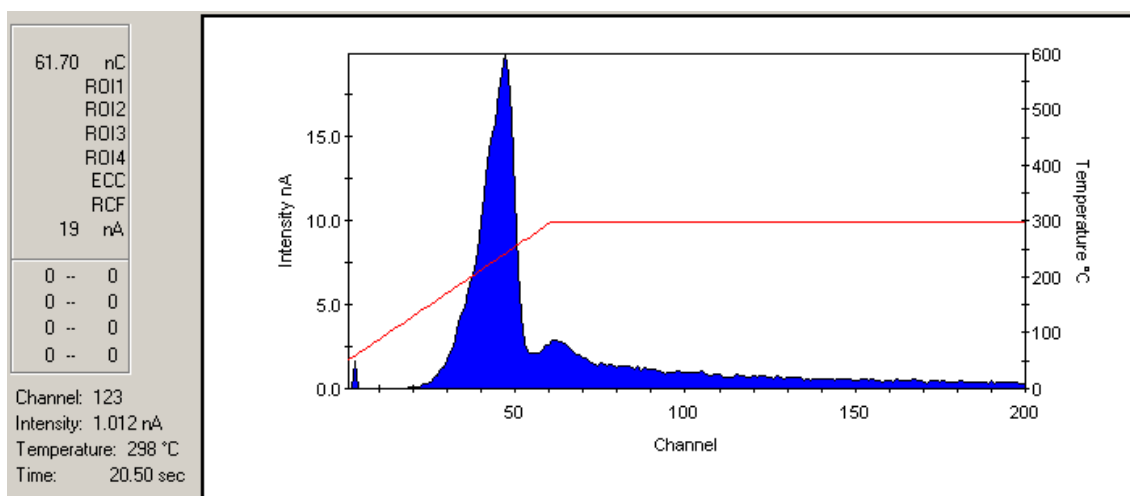
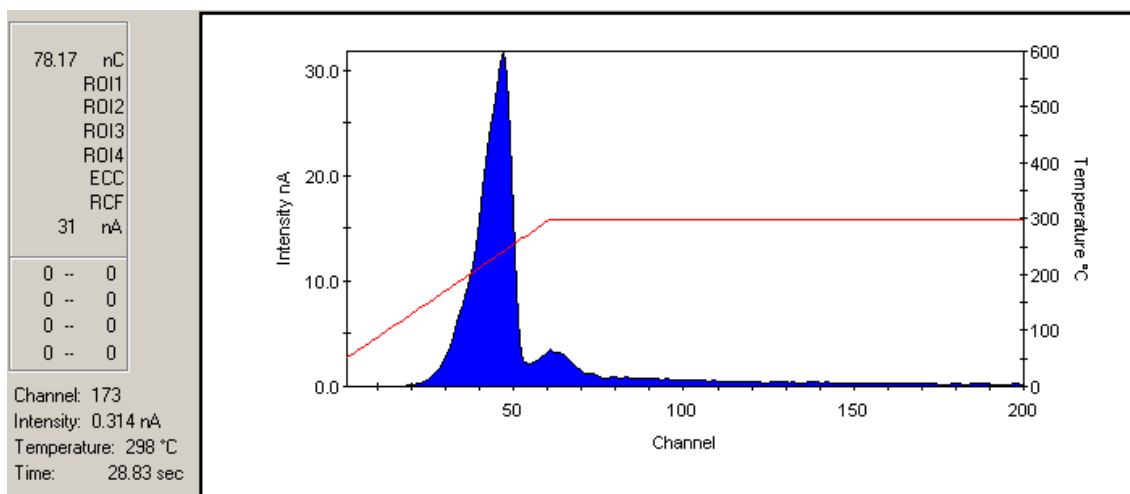
APPENDIX F

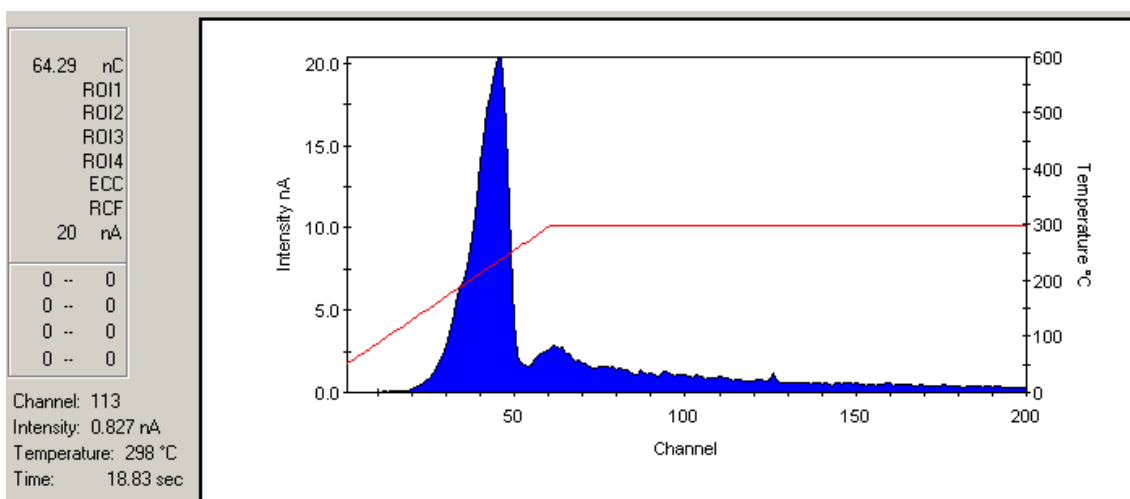
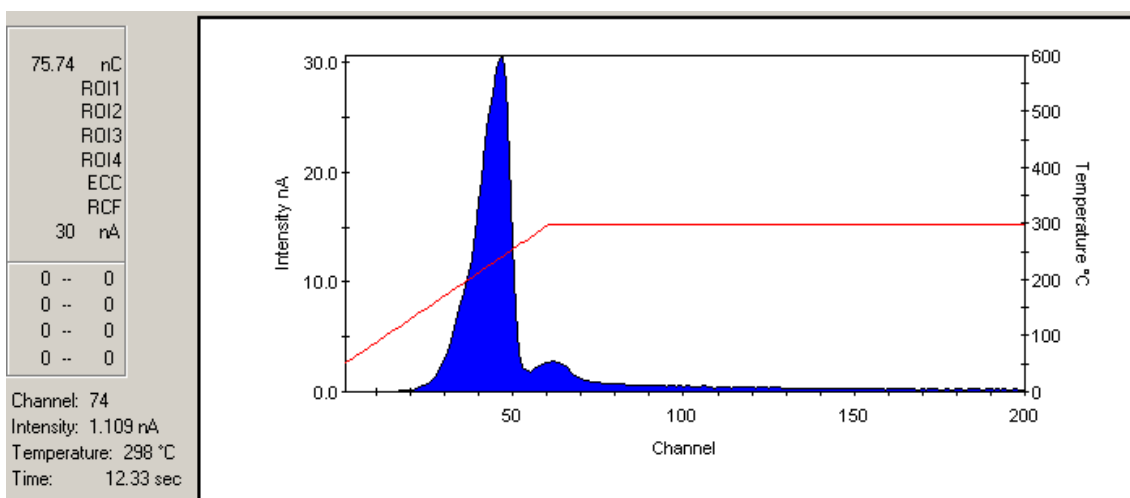
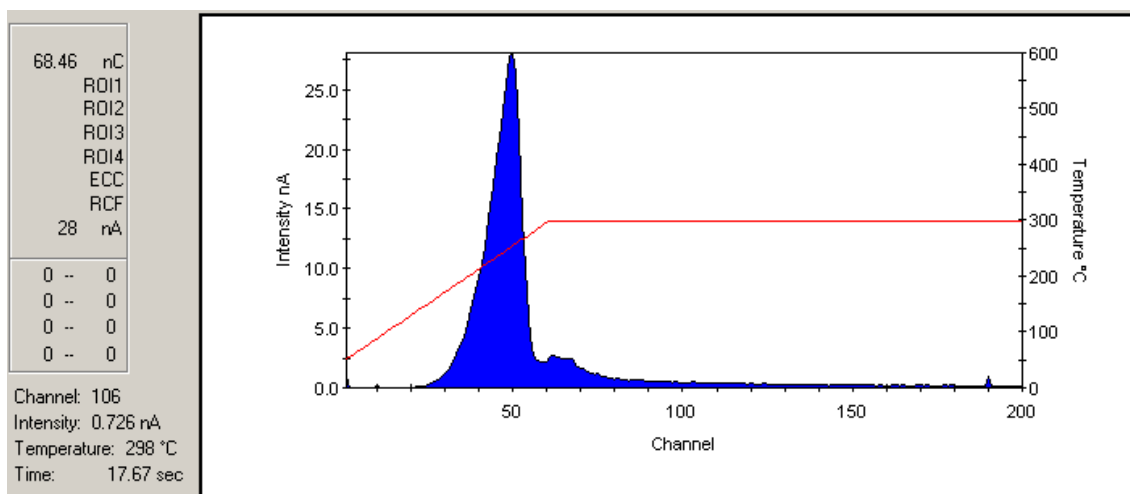
Calibration Glow Curves Generated by Exposing to 1.086 R X-Ray. Figures are Displayed in Order of TLD Number from 1 to 15.

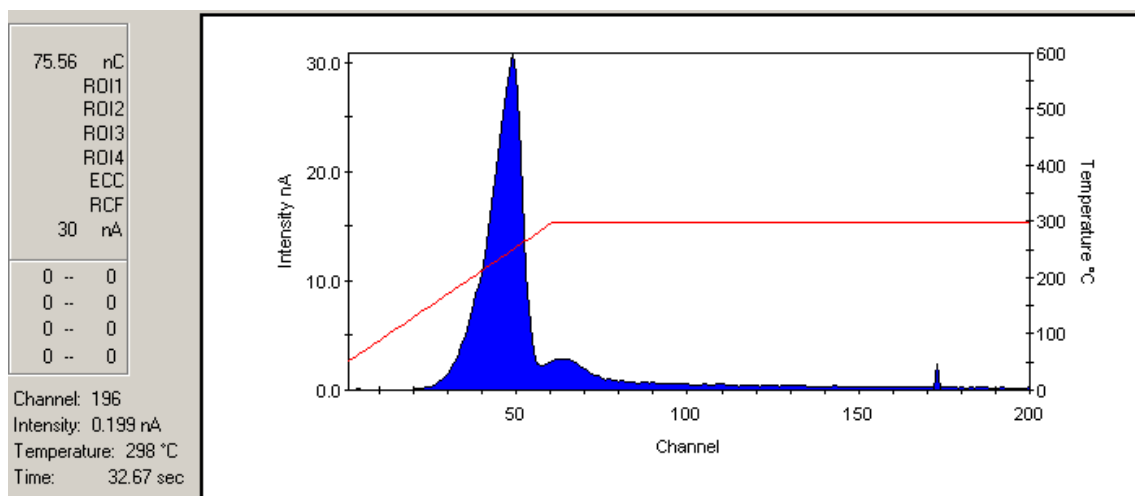












VITA

Name: Ruoming Bi

Address: Department of Nuclear Engineering, Texas A&M University, 3133
TAMU, College Station, TX 77843-3133

Email Address: ruomingbi@hotmail.com

Education: B.S., Radiological Health Engineering, Texas A&M University, 2008